# APOGEE Chemical Abundances of Stars in the MW Satellites Fornax, Sextans, Draco and Carina

Cheng Xu<sup>1,2</sup>, Yi Qiao<sup>1,2</sup>, Baitian Tang<sup>1,2</sup>, José G. Fernández-Trincado<sup>3</sup>, Zhiqiang Yan<sup>4,5</sup>, and Doug Geisler<sup>6,7</sup>

- Department of Astronomy, School of Physics and Astronomy, Sun Yat-sen University, Zhuhai, Guangdong Province, China e-mail: tangbt@sysu.edu.cn
- CSST Science Center for the Guangdong-Hong Kong-Macau Greater Bay Area, Zhuhai 519082, China
- Instituto de Astronomía, Universidad Católica del Norte, Av. Angamos 0610, Antofagasta, Chile
- School of Astronomy and Space Science, Nanjing University, Nanjing 210093, PR China
- Key Laboratory of Modern Astronomy and Astrophysics (Nanjing University), Ministry of Education, Nanjing 210093, PR China
- Departamento de Astronomía, Casilla 160-C, Universidad de Concepción, Concepción, Chile
- Departamento de Astronomía, Facultad de Ciencias, Universidad de La Serena. Av. Raúl Bitrán 1305, La Serena, Chile

#### **ABSTRACT**

During its evolution, the Milky Way (MW) incorporated numerous dwarf galaxies, particularly low-mass systems. The surviving dwarf galaxies orbiting the MW serve as exceptional laboratories for studying the unique properties of these systems. Their metalpoor environments and shallow gravitational potentials likely drive significant differences in star formation and star cluster properties compared to those in the MW. Using high-quality near-infrared spectra from the APOGEE survey, we determined abundances of Fe, C, N, O, Mg, Al, Si, Ca, Ti, Cr, Mn, Ni, and Ce for 74 stars in four MW satellite dwarf galaxies: Fornax, Sextans, Draco, and Carina. Our analysis reveals that the distribution of  $\alpha$  elements (e.g., [Si/Fe]) strongly correlates with galaxy luminosity (and hence mass), underscoring the critical role of galaxy mass in shaping chemical evolution. These dwarf galaxies exhibit [Al/Fe]  $\sim -0.5$ , which is comparable to those of the metal-poor stars in the MW. Additionally, we identified nitrogen-rich field stars in the Fornax dwarf galaxy, which display distinct metallicities compared to its known globular clusters (GCs). If these stars originated in GCs and subsequently escaped, their presence suggests we are observing relics of destroyed GCs, offering possible evidence of cluster disruption.

**Key words.** dwarf galaxies – chemical abundances – globular clusters

Portion of Astronomy, School of Physics and Astronomy, Semail: tangbt@sysu.edu.cn

2 CSST Science Center for the Guangdong-Hong Kong-Macau G

3 Instituto de Astronomy and Space Science, Nanjing University, Av. Ar. School of Astronomy and Space Science, Nanjing University, N

5 Key Laboratory of Modern Astronomy and Astrophysics (Nanji Departamento de Astronomía, Casilla 160-C, Universidad de Cc. 7 Departamento de Astronomía, Facultad de Ciencias, Universidad Received—,—; accepted—,—

ABST

During its evolution, the Milky Way (MW) incorporated numero dwarf galaxies orbiting the MW serve as exceptional laboratories poor environments and shallow gravitational potentials likely drive compared to those in the MW. Using high-quality near-infrared sp C, N, O, Mg, Al, Si, Ca, Ti, Cr, Mn, Ni, and Ce for 74 stars in four Our analysis reveals that the distribution of \$\alpha\$ elements (e.g., [Si/] underscoring the critical role of galaxy mass in shaping chemical comparable to those of the metal-poor stars in the MW. Additionall which display distinct metallicities compared to its known globula escaped, their presence suggests we are observing relics of destroy Key words. dwarf galaxies—chemical abundances—globular clusters in the first observed scaling relations, e.g., the mass-luminosity relation (e.g., Bell et al. 2003), and the mass-metallicity relation (e.g., Lequeux et al. 1979; Foster et al. 2012), play a pivotal role in deciphering galaxy formation and evolution across diverse cosmic environments characterized by variations in age, metallicity, and redshift. Nevertheless, the underlying physical mechanisms driving these processes remain subjects of ongoing scientific debate. In this context, the ability to resolve galaxies into their constituent stars provides the most direct observational approach for probing their assembly histories.

The hierarchical galaxy formation paradigm suggests that dwarf galaxies originate within dark matter subhalos, subsequently merging to assemble larger galactic systems like the Milk

quently merging to assemble larger galactic systems like the Milky Way (MW). This framework is observationally supported by the numerous dwarf satellites identified in the MW's vicinity (Hodge 1971, 1989; Grebel et al. 2003; Tolstoy et al. 2009; McConnachie 2012; Ibata et al. 2013; Weisz et al. 2014; Simon 2019). Recent discoveries have further revealed both tidally disrupting systems, such as the Sagittarius (Sgr) stream (Majewski et al. 2003; Law & Majewski 2010), and fully disrupted remnants including the Gaia-Sausage-Enceladus (GSE; Belokurov et al. 2018; Helmi et al. 2018), and the Sequoia (e.g., Myeong et al. 2019) substructures. These systems display remarkable diversity in mass distribution, morphological configuration, and

stellar population properties. Through comparative analysis with numerical simulations, they offer critical insights into halo assembly processes, the environmental regulation of galaxy formation, and their dynamical interactions throughout cosmic history.

The stellar chemical abundance patterns of galaxies serve as a fossil record of their evolutionary history. For example, stars in dwarf galaxies show systematically lower metallities than those of MW stars. Furthermore, the characteristic "knee" in the  $[\alpha/Fe]$ -[Fe/H] trend provides a diagnostic tool for estimating the star formation history in dwarf galaxies (e.g., Tinsley 1979; Shetrone et al. 2003; Kobayashi et al. 2006; Nidever et al. 2014; Kirby et al. 2020; Nidever et al. 2020). Building on this framework, Hasselquist et al. (2021) proposed the potential occurrence of a second starburst episode in several nearby MW satellite galaxies, inferred from chemical evolution modeling of their  $[\alpha/Fe]$ –[Fe/H] distributions. High-precision abundance measurements also enable investigations into variations in the stellar initial mass function (IMF) across galactic environments (e.g., McWilliam et al. 2013; Hasselquist et al. 2017; Carlin et al. 2018). These chemical signatures collectively offer critical insights into the diverse physical processes governing galaxy assembly and evolution.

Clustered star formation is ubiquitously observed across cosmic time, manifesting in both the low-redshift (low-z) Universe (Pace 2024) and the high-z Universe (e.g., Adamo et al. 2024). Surviving star clusters serve as crucial tracers of galactic star formation histories. These stellar systems are typically classified into open clusters and globular clusters (GCs), with the latter exhibiting distinctive chemical abundance patterns characterized by N, Na, and Al enhancements alongside C, O, and Mg depletion (Carretta et al. 2010; Milone et al. 2015; Mészáros et al. 2015; Bastian & Lardo 2018; Tang et al. 2017, 2018, 2021; Li et al. 2021) — a phenomenon recognized as multiple populations (MPs). Our ongoing research initiative, "Scrutinizing GAlaxy-STaR cluster coevolutiON with chemOdynaMIcs (GASTRONOMI)", employs multi-wavelength photometric and spectroscopic data to unravel the coevolutionary relationships between the MW, its satellite dwarf galaxies, and their stellar clusters. Recent analysis of MP detections in ancient star clusters by Huang et al. (2024) reveals two critical parameters governing MP formation: cluster compactness and metallicity. Intriguingly, this study found an absence of MPs in younger Sgr-associated clusters (<8 Gyr), contrasting sharply with their older counterparts. This disparity may reflect the metallicity evolution of the galactic environment, suggesting suboptimal conditions for MP formation in metalrich settings. Extending this investigation to the Sculptor dwarf galaxy (Scl), Tang et al. (2023, hereafter T23) reported no detectable GCs or chemically peculiar stars indicative of GC dissolution. Our modeling analysis of APOGEE chemical abundance data yields a top-light IMF for Scl, characterized by a high-mass slope of -2.7. This paucity of massive stars aligns with the observed dearth of compact star clusters, which typically serve as nurseries for high-mass star formation.

As GCs orbit their host galaxies, they gradually lose stars to the field population through dynamical processes, with some clusters eventually dissolving entirely. Identifying these GC escapees is important for modeling galaxy-star cluster interactions, yet their kinematic resemblance to halo stars makes them challenging to detect. Recent studies have uncovered a substantial population of nitrogen-rich (N-rich) field stars in the MW (e.g., Lind et al. 2015; Martell et al. 2016; Schiavon et al. 2017; Fernández-Trincado et al. 2016, 2017, 2019; Tang et al. 2019; Yu et al. 2021; Fernández-Trincado et al. 2022), which shared the most significant feature of MPs in GCs - N-enhancement. These stars are widely regarded as the strongest candidates for escaped GC members. Moreover, N-rich field stars have been detected in the Magellanic clouds (MCs) and Sgr (Fernández-Trincado et al. 2020, 2021), extending the evidence for GC dissolution to diverse galactic environments. By combining observations of extant GCs with their dispersed stellar remnants, we can construct a more complete picture of GC evolution, dissolution histories, and their role in shaping galactic stellar populations.

How do lower-mass Milky Way satellites contribute to our understanding of galactic chemical evolution? Can N-rich field stars be identified in these systems, and what do they reveal about the interplay between star cluster dynamics and galaxy evolution? In this study, we present detailed chemical abundance measurements for up to 13 elements across four dwarf spheroidal galaxies: Fornax (Fnx), Draco (Dra), Carina (Car), and Sextans (Sex). Section 2 outlines the data acquisition and reduction. In Section 3, we systematically compare abundance patterns for  $\alpha$ -elements (O, Mg, Si), iron-peak species (Cr, Mn, Ni), and neutron-capture elements (e.g., Ce), highlighting both commonalities and divergences across these satellite systems. We further examine radial abundance gradients and investigate the presence of N-rich field stars, discussing their potential origins and implications in Section 4. Finally, our conclusions and a summary of key findings are outlined in Section 5.

#### 2. Data Reduction

#### 2.1. Observational data

The near-infrared (H-band,  $\lambda = 1.51 - 1.69 \,\mu\text{m}$ ), high-resolution (R ~ 22,500) spectra are provided by the Apache Point Observatory Galactic Evolution Experiment (APOGEE, Majewski et al. 2017), which was part of the Sloan Digital Sky Survey III (SDSS-III, Eisenstein et al. 2011) and SDSS-IV (Blanton et al. 2017). The APOGEE survey were carried out with two telescopes: the 2.5 m telescope at the Apache Point Observatory (Blanton et al. 2017) and the 2.5 m du Pont telescope at the Las Campanas Observatory (Bowen & Vaughan 1973). The APOGEE survey sample primarily consists of red giant stars (RGB) across the MW (Majewski et al. 2017; Santana et al. 2021; Beaton et al. 2021). To date, APOGEE has observed nearly a million stars, covering the MW and neighboring galaxies. Furthermore, APOGEE data reduction software is used to simplify multiple 3D raw data cubes into well-sampled, calibrated combined 1D spectra (Nidever et al. 2015). Stellar parameters are derived using the FERRE code (Allende Prieto et al. 2006), which finds the best solution by comparing the observed spectra with the libraries of theoretical spectra (Zamora et al. 2015).

With 17 data releases of SDSS (DR 17, Abdurro'uf et al. 2022) to date, dwarf galaxies in the vicinity of the MW have been observed multiple times, and the signal-to-noise ratios (S/N) have reached a level sufficient for chemical analysis. In this work, we cross-matched the catalogs of Gaia Collaboration et al. (2018) and APOGEE DR17 to select potential member stars of Fnx, Dra, Car, and Sex dwarf galaxies. To reduce the uncertainties of derived chemical abundances, we excluded spectra with S/N < 70. Furthermore, we examined the radial velocities (RVs) of these candidates (Table 1), finding that the RVs of all member stars fall within  $3\sigma$  range. Therefore, the reliability of these member stars is confirmed by their spatial positions, proper motions, and RVs. There are 32 members in Fnx, 14 members in Dra, 19 members in Car, and 8 members in Sex. The locations of our Fnx sample stars and their positions in the color-magnitude diagram are plotted in Fig. 1.

#### 2.2. Stellar parameters and chemical abundances

In this work, we determined the photometric effective temperature ( $T_{\rm eff}$ ) using 2MASS photometry, following the method outlined by González Hernández & Bonifacio (2009). The final  $T_{\rm eff}$  values were derived from the dereddened color indices (J-K), using the extinction map from Schlegel et al. (1998). The surface gravity (log g) values were estimated from the canonical equation:

$$\log(\frac{g}{g_{\odot}}) = \log(\frac{M}{M_{\odot}}) + 4\log(\frac{T}{T_{\odot}}) - \log(\frac{L}{L_{\odot}})$$
 (1)

where the stellar mass is assumed to be 0.8 solar mass. To estimate the bolometric luminosities, we apply the bolometric correction procedure described by Alonso et al. (1999). The derived values of  $T_{\rm eff}$  and  $\log g$  are presented in Table 1. The uncertainties of  $T_{\rm eff}$  are dominated by those of the  $T_{\rm eff}$ -(J-K) relation, which is 94 K. The  $T_{\rm eff}$  uncertainties are propagated to the estimation of  $\log g$  uncertainties.

Chemical abundances under the assumption of local thermal equilibrium (LTE), were analyzed using the Brussels Automatic Stellar Parameter (BACCHUS) code (Masseron et al. 2016). Built upon the radiative transfer code, Turbospectrum (Alvarez & Plez 1998; Plez 2012), BACCHUS interpolates model atmospheres from the MARCS model grids (Gustafsson et al. 2008).

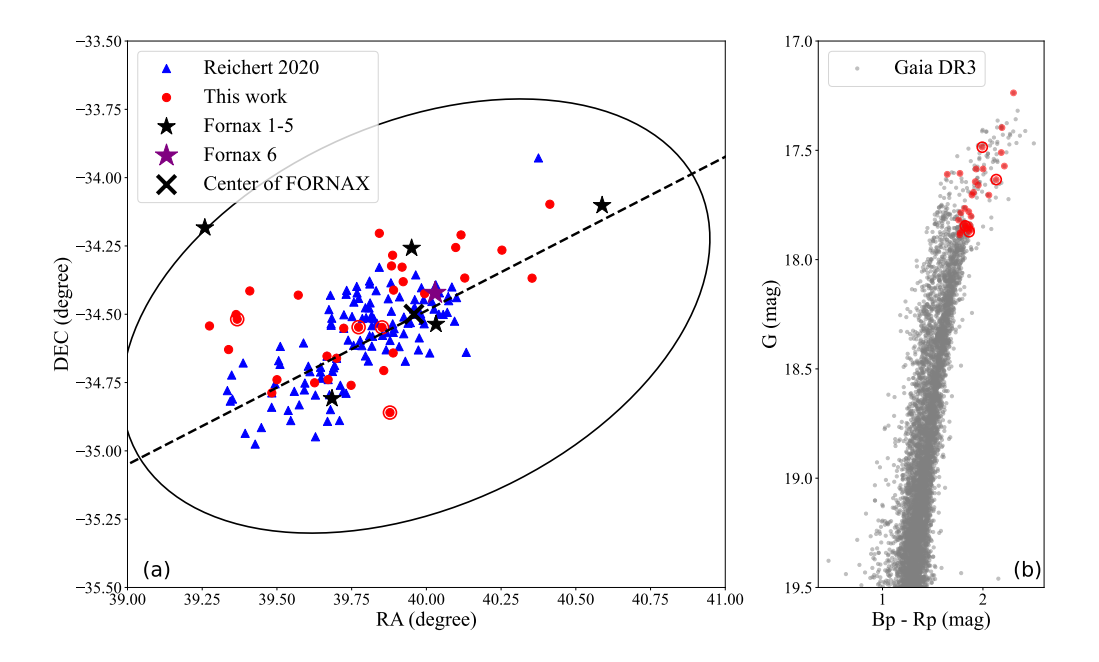


**Fig. 1.** Target information. (a): Spatial distribution of target stars in Fnx dwarf galaxy. The black ellipse indicates the tidal radius of Fnx and its center is labelled with black cross. Target stars from R20 and this work are marked as blue triangles and red dots, respectively. The N-rich stars are further marked with red circles. The black stars represent GC Fnx 1-5 while the purple star represents GC Fnx 6. (b): Color–magnitude diagram of Fnx stars based on *Gaia DR3* (grey dots).

Table 1. Basic information of our sample stars

#	APOGEE ID	RA [deg]	DEC [deg]	T <sub>eff</sub> [K]	log g	<i>RV</i> [km s <sup>-1</sup> ]	S/N	Gmag [mag]	BP-RP [mag]	Dwarf Galaxy
1	2M02403081-3422028	40.12842	-34.36745	3626	0.35	81	83	17.61	1.77	Fnx
2	2M02372118-3437451	39.33825	-34.62923	3845	0.74	63	112	17.59	1.93	Fnx
3	2M02392578-3442220	39.85744	-34.70617	3586	0.27	59	130	17.40	2.19	Fnx
4	2M02402354-3415204	40.09813	-34.25565	3552	0.24	36	96	17.70	2.06	Fnx
5	2M02413913-3405505	40.41308	-34.09736	3684	0.56	59	79	17.84	1.82	Fnx
6	2M02381712-3425482	39.57135	-34.43009	3696	0.56	54	114	17.51	2.18	Fnx
7	2M02410066-3415551	40.25277	-34.26532	3796	0.72	57	80	17.78	1.86	Fnx
8	2M02380004-3444219	39.50015	-34.73947	3806	0.75	40	85	17.80	1.88	Fnx
9	2M02372718-3430033	39.36329	-34.50095	4012	0.97	50	72	17.86	1.79	Fnx
10	2M02390557-3432503	39.77323	-34.54732	4054	1.01	57	76	17.85	1.83	Fnx
	•••	•••	•••	•••	•••	•••	•••	•••	•••	•••

Notes. Full table at the CDS.

The code's meticulous line selection and inspection capabilities were essential for analyzing the weak spectral lines characteristic of the metal-poor stars in our sample. For each absorption line, the abundance derivation began with a sigma-clipping selection of continuum regions, followed by a linear fit. This step identifies and rejects poor fits caused by features like bad pixels or abrupt spectral drops. The abundance is then estimated by comparing the observed and synthetic spectra using four independent methods: (1)  $\chi^2$  minimization of the overall fit; (2) comparison of the line core intensity; (3) equivalent width analysis; and (4) spectral synthesis (see Fig. 12 of Yu et al. 2021). Each method is assigned a quality flag. To ensure robustness, we only accepted an abundance measurement if all four methods yielded a satisfactory fit; otherwise, the line was rejected.

Given the prevalence of CO, CN, and OH molecular lines in the APOGEE spectral range, we determined the abundances of C, N, O, and Fe in a self-consistent, iterative procedure to account for their interdependencies, following Smith et al. (2013). We first derived the oxygen abundance from <sup>16</sup>OH lines, then carbon from <sup>12</sup>C<sup>16</sup>O, and nitrogen from <sup>12</sup>C<sup>14</sup>N, before determining the iron abundance from Fe I lines. With these key elements established, we performed a line-by-line analysis of atomic lines for Mg, Al, Si, Ca, Ti, Cr, Mn, Ni, and Ce. While strong lines for Mg, Al, and Si allowed for a comprehensive analysis, many lines for Cr, Mn, Ni, and Ce, as well as some molecular <sup>12</sup>C<sup>16</sup>O and <sup>12</sup>C<sup>14</sup>N lines, were too weak for reliable measurement. These were carefully inspected and excluded from the final abundance set. The resulting chemical abundances are presented in Table 3, with solar abundances adopted from Asplund et al.

(2005) as our reference. Other elements, such as sodium (Na), were not analyzed due to their weak and unreliable absorption lines in our data.

We first estimated the uncertainties of chemical abundances caused by individual stellar parameter error:  $\sigma_{\Delta T_{\rm eff}}, \sigma_{\Delta \log g}$ , and  $\sigma_{\Delta [{\rm Fe/H}]},$  where their typical errors were set as:  $\Delta T_{\rm eff}=100~{\rm K},$   $\Delta \log g=0.25$  dex. Subsequently, the total estimated error is:  $\sigma_{\rm tot}=[(\sigma_{\Delta T_{\rm eff}})^2+(\sigma_{\Delta \log g})^2+(\sigma_{\Delta [{\rm Fe/H}]})^2]^{1/2}.$  The errors for Star #10 are shown in Table 2 as an example.

### 3. Results

#### 3.1. $\alpha$ -elements

According to nucleosynthetic models (Kobayashi et al. 2020),  $\alpha$ -elements are primarily synthesized in exploding massive stars (Type II supernovae, SNe II), while iron is produced by both Type Ia supernovae (SNe Ia) and SNe II. Since the timescale of SNe II ( $\sim$  Myr) is much shorter than that of SNe Ia ( $\sim$  100 Myr), the interstellar medium (ISM) is contaminated by  $\alpha$ -rich materials at earliest time. Therefore, high  $\alpha$  abundances are generally observed in low metallicity stars. After the onset of SNe Ia, so-called 'SNe Ia delay time', the ejection of large amounts of iron continues to increase the [Fe/H], but decreases the [Mg/Fe] of the ISM and thus the later formed stars. This point of decline, termed the "knee" in the  $[\alpha/\text{Fe}]$  versus [Fe/H] trend, is influenced by the galaxy's star formation rate (SFR) and mass: generally the  $\alpha$  knee appears at a lower metallicity in lower mass galaxies since they have a lower SFR (Tolstoy et al. 2009).

The relationship between  $[\alpha/Fe]$  and [Fe/H] is illustrated in Fig. 2, where background data include stars from the Galactic halo, disk, and dwarf galaxies. For each galaxy, we generally see a relatively constant  $[\alpha/Fe]$  at low metallicity, which begins to decline above a certain metallicity, commonly referred as the  $\alpha$  knee. However, the data are more complex than expected due to the uncertainties and systematics. The Ti abundance measurements show larger dispersion due to the relatively weak absorption lines. Meanwhile, the O abundances also present a fairly large scattered distribution, particularly for metal-poor stars, which could be attributed to their iterated derivation procedures between C, N, O related molecular lines needed to achieve molecular equilibrium (T23). Note that a few metal-rich Fnx stars ([Fe/H] > -0.75) show relatively high [O/Fe], probably due to their AGB nature with enhanced [Ce/Fe] (See Section 3.4). Our measured Mg abundances are systematically lower (~ 0.2 dex) than those derived from the optical spectra, as we pointed out before. Interestingly, a large portion of stars in Sex show low [Mg/Fe] ( $\sim -0.6$ ), which may be related to the second knee implied by R20. We will further discuss the correlation between galaxy mass and  $\alpha$ -element distribution in Section 4.2.

# 3.2. Odd-Z element: Al

Al is primarily synthesized in massive stars (Arnett 1971; Woosley & Weaver 1995) and is released into the ISM via SNe II. Its yield may depend on the metallicity of the progenitor stars (e.g., Weinberg et al. 2019). Al also can be generated via high temperature hydrogen burning through the Mg-Al cycle (Arnould et al. 1999), which can be found in stellar objects like Wolf-Rayet stellar winds (Limongi & Chieffi 2006) and AGB

As shown in Fig. 3, the Al abundances of our studied dwarf galaxies are systematically lower than those from the MW disk ([Fe/H] > -1.5). However, they are comparable to some MW

halo stars ([Fe/H] < -1.5). It is speculated that the early evolution of [Al/Fe] is similar between a MW-like galaxy and a GSE-like galaxy (Horta et al. 2021). No clear trend is seen in Car, Dra, and Sex, given that the sample size of each dwarf galaxy is small. We do find a vague trend that [Al/Fe] of Fnx stars decreases with increasing metallicity in the more metal-poor regime ([Fe/H] < -0.75), but start flattening in the more metal-rich regime. This possible flattening feature is also vaguely found in [Mg/Fe] and [Si/Fe]. Hasselquist et al. (2021) suggests such a feature is caused by a secondary burst of star formation.

#### 3.3. Iron-peak elements

Analyses of solar elemental abundances reveal that iron-peak elements are actually contributed by both SNe Ia and core-collapse SNe II (Woosley & Weaver 1995). Due to differences in star formation timescales and histories between the MW and dwarf galaxies, the iron-peak element abundances also vary accordingly.

The atomic lines for Cr, Mn, and Ni are relatively weak in the APOGEE spectra, making it impossible to obtain abundances for all sample stars. [Cr/Fe] generally shows a flat trend as a function of metallicity for MW, Sgr, and Fnx (Fig. 5). The Sgr and Fnx stars show greater dispersion in Cr, especially for more metalpoor stars, probably due to their weaker lines and lower SNR in the NIR spectra.

For MW and Sgr, [Mn/Fe] are almost constant ( $\sim -0.3$ ) in the range of [Fe/H] < -1.0, and increase in the more metalrich regime. Based on the limited measurements, Car stars show a similar flat trend ( $\sim -0.2$ ) as a function of metallicity for [Fe/H] < -1.0; Fnx stars show similar [Mn/Fe] values as Sgr stars between -1.0 < [Fe/H] < -0.6. However, it is difficult to tell its trend with metallicity given the limited metallicity range and large scatter.

No obvious [Ni/Fe] trend is found in the metal-poor regime ([Fe/H] < -1.3) for any aforementioned galaxies, due to their large abundance scatter. However, in the metal-rich regime ([Fe/H] > -1.3), Sgr stars show lower [Ni/Fe] compared to MW stars, and Fnx stars seem to show even lower values. In this regime, [Ni/Fe] decreases as the metallicity increases. Similar results are found in the optical counterpart (R20). Theoretical studies suggest a significant contribution of sub-Chandrasekhar mass channels to SNe Ia in Fnx, possibly with additional progenitor mass variation related to star formation history (Sanders et al. 2021; Nissen et al. 2024).

#### 3.4. Neutron-capture elements: Ce

Elements heavier than iron are generally formed through neutron-capture processes, which are classified into rapid (r-) and slow (s-) neutron-capture processes depending on the relative rates of neutron capture and  $\beta$ -decay. For several decades, the astrophysical sites of these processes have been the subject of ongoing research and debate. For the r-process, current mainstream models include core-collapse SNe (e.g., Woosley et al. 1994) and neutron star mergers (e.g., Côté et al. 2018; Watson et al. 2019). The s-process, on the other hand, primarily occurs in AGB stars during thermal pulsation phases (Busso et al. 2001; Karakas & Lattanzio 2014). According to Bisterzo et al. (2014), approximately 83% of the Ce in our Sun originates from the s-process, which is similar to another frequently measured s-process-dominated element, Ba (85%).

Table 2. Errors of chemical abundances propagated from atmospheric parameters for star #10.

Element	$\Delta T_{\rm eff} = 100  ({ m K})$	$\Delta \log(g) = 0.25  (\text{dex})$	$\Delta[\text{Fe/H}] = 0.1 (\text{dex})$	$\sigma_{ m tot}$
[C/Fe]	0.251	0.357	0.292	0.525
[N/Fe]	0.282	0.385	0.279	0.553
[O/Fe]	0.189	0.092	0.012	0.211
[Mg/Fe]	0.154	0.173	0.129	0.265
[Al/Fe]	0.102	0.074	0.015	0.127
[Si/Fe]	0.008	0.025	0.009	0.028
[Ca/Fe]	0.064	0.164	0.021	0.177
[Ti/Fe]	0.865	0.142	0.798	1.185
[Cr/Fe]	0.134	0.226	0.025	0.264
[Mn/Fe]	0.015	0.138	0.042	0.145
[Ni/Fe]	0.010	0.023	0.054	0.060
[Ce/Fe]	0.051	0.032	0.047	0.076

Table 3. Chemical abundances

#	[Fe/H]	[C/Fe]	[N/Fe]	[O/Fe]	[Mg/Fe]	[Al/Fe]	[Si/Fe]	[Ca/Fe]	[Ti/Fe]	[Cr/Fe]	[Mn/Fe]	[Ni/Fe]	[Ce/Fe]	Dwarf Galaxy
1	-1.65	•••	•••	-0.13	0.11	-0.47	0.28	0.15	•••	•••	•••	•••	•••	Fornax
2	-1.32	•••	•••	•••	•••	-0.89	-0.08	•••	•••	•••	•••	•••	-0.07	Fornax
3	-1.21	0.45	0.56	0.35	0.29	-0.42	0.39	0.14	0.04			0.11	0.19	Fornax
4	-1.12	•••	•••	0.05	-0.09	-0.81	0.07	-0.09	-0.51	•••	-0.16	•••	0.14	Fornax
5	-1.1	•••	•••	-0.31	-0.05	-0.43	0.18	0.04	0.22	-0.27	-0.04	•••	0.26	Fornax
6	-1.07	0.05	-0.13	0.27	-0.07	-0.5	0.11	0.09	-0.24	-0.33	-0.15	-0.01	0.18	Fornax
7	-1.04	-0.47	0.36	-0.06	•••	-0.46	0.03	-0.01	0.15	0.03	-0.25	•••	0.32	Fornax
8	-1.01	-0.13	0.07	0.21	•••	-0.8	0.12	-0.03	-0.29	-0.15	-0.17	0.09	0.32	Fornax
9	-0.99	•••	•••	0.47	-0.13	-0.32	0.15	0.24	0.14	0.14	-0.09	-0.37	0.46	Fornax
10	-0.98	-0.52	1.23	0.46	-0.19	-0.38	-0.05		0.0	-0.14	-0.32		0.07	Fornax
•••		•••	•••	•••	•••	•••	•••	•••	•••	•••	•••	•••	•••	

**Notes.** Full table at the CDS.

Six stars show exceptionally large [Ce/Fe], including four from Fnx, one from Car, and one from Dra (Fig. 7). The usually large [Ce/Fe] indicate that they are possible AGB stars. This is further confirmed by their higher values of [N/Fe] and [O/Fe] when available (see T23 for further discussion). These AGB candidate stars do not seem to show abnormal values in other investigated elements of this work. After excluding the AGB candidates, we do not find significant [Ce/Fe] trend as a function of metallicity for all four dwarf galaxies, partially due to the large scatter in measured abundances. Notably, Ba, an element with similar s-process contribution as Ce, are measured in these four dwarf galaxies by R20. [Ba/Fe] generally show a flat trend as a function of metallicity for these dwarf galaxies between -2.3 < [Fe/H] < -0.5, which is consistent with the null [Ce/Fe] trend in this work.

### 4. Discussion

# 4.1. Comparison with literature and NLTE effects

In this section, we try to verify our derived abundances and look for possible systematics by comparing with abundances derived from the optical counterparts. Here we pick the work of (Reichert et al. 2020, hereafter R20), which derived abundances of 380 stars in 13 dwarf galaxies with archival optical high-resolution spectra. There are twelve common stars between our and their works. The top panels of Fig. 6 indicate that the stellar parameters generally agree with each other between two studies, although our derived log g values are slightly larger ( $\sim 0.3 \text{ dex}$ )

than those reported by R20. The middle and bottom panels of Fig. 6 show the comparisons of element abundances derived by two studies. Some stars may not have Cr, Mn, or Ni measurements, as they have weaker lines in the NIR wavelength range. Though with significant scatters ( $\sim 0.3 - 0.4$  dex), the derived element abundances agree with each other, except for Mg.

Our Mg abundances are systematically lower (approximately 0.2 dex) compared to those in R20. A similar trend is also found in T23, who suggests non-local thermodynamic equilibrium (NLTE) corrections for the adopted NIR Mg lines ( $\lambda \sim 15741, 15749, 15766$  Å) at the resolution of APOGEE spectra (Osorio et al. 2020; Masseron et al. 2021).

The NLTE corrections for aluminum abundances measured by APOGEE are generally negative, ranging from about –0.1 to –0.2 dex for RGB stars. These corrections vary depending on the specific spectral lines used and the stellar parameters, but they do not significantly alter the separation between different stellar populations (Feltzing & Feuillet 2023). Thus, while individual stellar abundances may be affected, the overall chemical trends found in this work remain robust.

The Mn I lines in H band originate from high-excitation levels and are relatively sensitive to departures from LTE especially in the metal-poor giants (Amarsi et al. 2020). The primary direction of the NLTE correction is positive. For metal-poor stars with [Fe/H] < -1.0, these corrections can reach between +0.2 dex and +0.5 dex (in extreme cases). Applying these NLTE corrections may raise the [Mn/Fe] ratios

at low metallicities, possibly resulting in a flatter and potentially plateau-like trend in the [Mn/Fe] vs. [Fe/H] plane.

#### 4.2. Galaxy mass and $\alpha$ -element

It is suggested that the more massive galaxy is more metal-rich with faster star formation enrichment (e.g., Tinsley 1979; Tolstoy et al. 2009). This relation may be complicated by the lost mass in tidally disrupted galaxies (Tolstoy et al. 2009). However, it generally reflects that more mass galaxies have longer star formation history (SFH) due to their strong potential well, and thus forming more metal-rich stars with low  $[\alpha/Fe]$ . In this work, we collect the data of MW, Sgr, Scl, Fnx, Car, Dra, and Sex to find the rough correlation between the trend of  $\alpha$ -element and luminosity which is a proxy for galaxy mass. Given that O, Ca, Ti show larger scatters, and Mg may be systematically lower than those from the optical, we use Si as the tracer of  $\alpha$ -element (Fig. 4). Limited by the sample sizes and metallicity coverage of each galaxy, accurate estimation of the  $\alpha$ -knee, if any, could be tricky. Instead, we perform a polynomial fit to the distribution of [Si/Fe] vs. [Fe/H] for each dwarf galaxy (Fig. 4), and find out their intersection with [Si/Fe] = 0 (Table 4). Clearly, the more luminous, and thus more mass galaxies (Table 4) show more metal-rich metallicities at the intersection, underscoring the critical role of galaxy mass in shaping chemical evolution. Interestingly, we find that the brightest galaxies, i.e., Sagittarius and Fornax, show similar metallicities at the intersection, suggesting they may have comparable masses in the past, and thus similar chemical evolution.

#### 4.3. Radial chemical gradients

Radial chemical gradients are important observational constraints to reconstruct galaxy formation history (Magrini et al. 2017). The sample sizes of Dra, Car, and Sex are not large enough for meaningful discussions, and we focus on Fnx in this section. Being one of the first dwarf spheroidals discovered by Harlow Shapley in 1938, Fnx has been investigated for a long time. Fnx shows a prolonged star formation history, with at least three distinct stellar populations: a young population (few 100 Myr old), an intermediate age population (2-8 Gyr old), and an ancient population (> 10 Gyr, Battaglia et al. 2006). The stellar populations in Fnx can be separated into two/three components considering their spatial, kinematics and metallicity distributions: the metal-rich component is more centrally concentrated with colder kinematics, and vice versa (Battaglia et al. 2006; Walker & Peñarrubia 2011; Amorisco & Evans 2012). These components show misalignment between their angular momentum vectors and different anisotropy parameters (Amorisco & Evans 2012; Kowalczyk & Łokas 2022), indicating a "core" dark matter density profile (Walker & Peñarrubia 2011), and a late merger history (Amorisco & Evans 2012).

Chemical abundance investigation is more challenging, since it demands spectra with higher SNR (Shetrone et al. 2003; R20). Hasselquist et al. (2021) suggests a second, weaker "burst" star formation in Fnx based on chemical modelling the [ $\alpha$ /Fe]-[Fe/H] patterns, in agreement with results from the color-magnitude diagram. As chemical abundances are strongly affected by galaxy star formation history, here we explore the possible radial chemical gradient in Fnx for the first time. We used linear least-squares regression fitting to find the correlations between chemical abundances and elliptical galactic radius. We list the results

in Table 5, including their slopes (k), slope errors, and p-value<sup>1</sup>. Our results suggest a nondetectable radial gradient for [O/Fe], [Mg/Fe], [Al/Fe], [Si/Fe], [Ca/Fe] and [Ti/Fe], given their twosided p-values are too large (> 0.05). However, we confirmed the metallicity gradient (p-value = 0.0004 and k = -0.7814, Fig. 8) suggested in literature (Battaglia et al. 2006; Amorisco & Evans 2012), where we further include stars with 40 < SNR (per pixel) < 70. If we divide them with [Fe/H] = -1 according to Kowalczyk & Łokas (2022), we find the average radius of the metal-rich stars is 0.1-0.2 degree, while it is 0.3-0.4 degree for their counterparts. This agrees with Battaglia et al. (2006, Fig. 15). The lack of detectable radial chemical gradients could be attributed to the following reasons: 1. Not large enough sample size (32 Fnx stars); 2. Measurement uncertainties and offsets ( $\sim 0.1 - 0.2$  dex); 3. Three star-formation epochs and possible merger history may form more complicated radial chemical gradients. When a new large-scale SF event occurs, one would expect the  $[\alpha/\text{Fe}]$  to increase after the first new SNe II and for the first 0.1-1 Gyrs until SNe Ia kick in, complicating any abundance gradient using  $\alpha$ -elements. We speculate the last one may be the driving factor: radial gradients of [Mg/Fe] and [Ca/Fe] were identified in Scl (T23), which formed most of the stars early with a single peak (de los Reyes et al. 2022).

#### 4.4. N-rich field stars

As part of our on-going project "GASTRONOMI", we aim to investigate the connection between star cluster properties and galaxy chemical evolution in these lower mass MW satellites. A substantial number of the existing MW GCs were born ex-situ, and later joined other in-situ GCs by mergers (e.g., Massari et al. 2019). GCs are also found in large MW satellite galaxies (e.g., LMC and SMC) and smaller dwarf galaxies (Huang & Koposov 2021). Many GCs are dissolved after birth (Li & Gnedin 2019), while member stars of surviving GC may escape its potential well through two-body relaxation. Therefore, GC escapees are expected to be found in the field. Using the chemical anomaly found in GCs, astronomers identified N-rich field stars as possible candidates for GC escapees. These stars can be found in dissolved dwarf galaxies (e.g., GSE, Yu et al. 2021), dissolving dwarf galaxies (e.g., Sgr, Fernández-Trincado et al. 2021), and existing dwarf galaxies (e.g, LMC & SMC, Fernández-Trincado et al. 2020).

Next, we try to identify N-rich field stars in Fnx, Dra, Car, Sex dwarf galaxies with the following criteria: [N/Fe] > 0.65, [C/Fe] < 0.15, and [Ce/Fe] < 0.5. Here we exclude stars with high C and Ce abundances to avoid AGB star contamination (Schiavon et al. 2017; Fernández-Trincado et al. 2019). We identify 4 N-rich field stars out of 32 sample stars (4/32) in Fnx, 0/14 in Dra, 0/19 in Car, and 0/8 in Sex. Considering that the effects of internal mixing in giant stars could also cause high N surface abundances, we compared the C&N abundances of these N-rich stars with the stellar models mentioned in Lagarde et al. (2012) (see Fig.9). Models including thermohaline convection and rotation-induced mixing are considered here. The systematically higher N and lower C abundances in our stars (particularly the two stars with [N/Fe] > +0.94) compared to the mixing models cannot be fully explained by internal processes like rotational or thermohaline mixing. Instead, such stars are more likely to be formed from gas previously enriched by the CNO-processed ejecta of massive first-

<sup>&</sup>lt;sup>1</sup> A hypothesis test is performed to assess whether the slope equals zero, using the Wald Test with a t-distribution for the test statistic.

**Table 4.** The metallicities at [Si/Fe] = 0 and absolute magnitudes for dwarf galaxies.

Galaxy	$[Fe/H]_{[Si/Fe]=0}$	$M_V [mag]^a$
Sgr	$-0.55 \pm 0.16$	$-13.5 \pm 0.30$
Fnx	$-0.62 \pm 0.15$	$-13.46 \pm 0.14$
Scl	$-1.08 \pm 0.11$	$-10.82 \pm 0.14$
Car	$-1.35 \pm 0.23$	$-9.43 \pm 0.05$
Sex	$-1.71 \pm 0.27$	$-8.72 \pm 0.06$
Dra	$-1.72 \pm 0.25$	$-8.71 \pm 0.05$

Notes. <sup>a</sup>: From McConnachie (2012) and Muñoz et al. (2018).

Table 5. Results of linear least squares regression for Fnx

-			
element	k	k error	p-value
	(dex/degree)	(dex/degree)	
[Fe/H]	-0.7814	0.217	0.0004
[O/Fe]	-0.2480	0.488	0.615
[Mg/Fe]	-0.1475	0.221	0.510
[Al/Fe]	-0.2178	0.229	0.351
[Si/Fe]	0.0687	0.149	0.647
[Ca/Fe]	-0.1202	0.215	0.581
[Ti/Fe]	0.2733	0.390	0.489

Notes. k: best-fit slope. p-value: two-sided p-value for a hypothesis test in which the null hypothesis is that the slope is zero.

# generation stars, imprinting high N and low C abundances at birth.

Additionally, N-rich field stars may show abnormal abundances in other elements, e.g., Al (Yu et al. 2021; Fernández-Trincado et al. 2021). However, we do not find such peculiarity in the four N-rich field stars of Fnx. Specifically, none of them show Al enrichment, which does not contradict the hypothesis that they are escaped from GCs —- more metal-rich GCs usually do not show Al enrichment (Pancino et al. 2017). The lack of N-rich field stars in Dra, Car, and Sex is not surprising, as similar situation is found in Scl (T23). It is probable that the low-mass, diffuse galactic environment is not suitable for the formation of GCs (Huang et al. 2024), and therefore should not have any N-rich field stars if they were formed in GCs.

Fnx shows not only a special chemodynamical structure (Section 4.3), but also remarkably high GC specific frequency<sup>2</sup>,  $S_N = 26$ . This value is exceptionally high among local galaxies, but it is comparable to those found in dwarf galaxies of the Coma cluster (Forbes et al. 2020). Currently, six GCs are suggested to be associated with Fnx (e.g., see Wang et al. 2019; Pace et al. 2021 and references therein), where three of them, Fnx 1 ([Fe/H] =  $-2.5 \pm 0.1$ ), Fnx 2 ([Fe/H] =  $-2.1 \pm 0.1$ ), Fnx 3 ([Fe/H] =  $-2.4 \pm 0.1$ ), show MPs, i.e., star-to-star variations in O, Na, and Mg (Letarte et al. 2006). Moreover, Fnx 3 ([Fe/H] =  $-2.28 \pm 0.02$ ), Fnx 4 ([Fe/H] =  $-1.24 \pm 0.02$ ), and Fnx 5 ([Fe/H] =  $-2.06 \pm 0.03$ ) were investigated by integrated-light spectra (Larsen et al. 2022). Fnx 6 is the most metal-rich one with [Fe/H] =  $-0.71 \pm 0.05$  (Pace et al. 2021).

Given the metallicity range of our measured Fnx stars, we plot the abundances of Fnx 3, Fnx 4, and Fnx 5 (Larsen et al. 2022) in Fig. 2 and 5 to visualize the abundance trend at lower

metallicities. With similar metallicity, Fnx 4 perfectly matches with our Fnx field stars in all measured abundances. Fnx 3 and Fnx 5 also match with other Fnx field stars in elements heavier than Ca, but lower [Mg/Fe] and higher [Si/Fe] are spotted when compared with field stars of other galaxies (e.g., MW). These peculiar features are in fact related to their GC nature: 1. The star-to-star Mg variation with depleted values is found in Fnx 3 (Letarte et al. 2006), where a similar situation may also be true in Fnx 5; 2. Enhanced Si abundances are commonly found in metal-poor Galactic GCs (e.g., Tang et al. 2018). Therefore, the enhanced Si integrated-light abundances indicate the existence of star-to-star Si variation with elevated values in Fnx 3 and Fnx 5. Our identified N-rich field stars show metallicity between -0.8and -1.0 (Table A.2) with measurement uncertainties of  $\sim 0.1$ dex. They do not overlap with any existing Fnx GCs either in metallicity or in spatial location (Fig. 1). Assuming that N-rich field stars are escaped from GCs (Tang et al. 2020; Yu et al. 2021), this may indicate GC destruction in Fnx. In fact, Chen & Gnedin (2023) predicted the number of GCs drops by a factor of  $\sim 5-8$  compared to the peak value based on modeling massive satellites with similar properties as Fnx. Therefore, the existence of GC escapees is expected by theoretical models. To further verify the destruction rate, a complete census of Fnx stars with high accurate abundances is needed.

#### 5. Summary

Although dwarf galaxies outnumber bright galaxies, their low surface brightness makes them challenging to observe in the distant Universe. The satellite dwarf galaxies orbiting the MW serve as ideal laboratories for studying the detailed evolution of galaxy systems. Specifically, we can model their evolution using resolved stellar populations in color-magnitude diagrams and their

<sup>&</sup>lt;sup>2</sup> The number of GCs per unit galaxy luminosity, i.e.,  $S_N = N_{GC} \times 10^{(M_V+15)}$ .

chemical abundances. Additionally, we can investigate the coevolution of galaxies and star clusters, as these systems mutually influence one another (Huang et al. 2024). Following our initial study of the Scl dwarf galaxy, this paper represents our second investigation into low-mass MW satellites using high-resolution spectra. We derived chemical abundances for Fe, C, N, O, Mg, Al, Si, Ca, Ti, Cr, Mn, Ni, and Ce in 74 member stars across the Fnx, Dra, Car, and Sex dwarf galaxies. To address the weak spectral lines in these metal-poor stars, we determined abundances line-by-line using the Turbospectrum wrapper — Bacchus.

- The  $\alpha$  elements (O, Mg, Si, Ca, Ti) exhibit a characteristic "flat then decreasing" trend with increasing metallicity. Given the smaller uncertainties and negligible systemic offset display by Si, the distribution of [Si/Fe] shows a strong correlation with the absolute magnitudes of galaxies (including Sgr, Scl and four dwarf galaxies in this work), confirming the critical role of galaxy mass in shaping chemical evolution.
- Al abundances in the studied dwarf galaxies cluster around [Al/Fe]~ -0.5, consistent with values observed in the Sgr dwarf galaxy or MW metal-poor stars. While Car, Dra, and Sex show no discernible metallicity-dependent trends, Fornax displays a tentative flattening of [Al/Fe] near [Fe/H]~ -0.75 after an initial decline with increasing metallicity.
- Leveraging Fnx's larger stellar sample, we investigated radial chemical abundance gradients. While confirming the previously reported metallicity gradient, we detected no significant radial trends for O, Mg, Al, Si, Ca, or Ti. This may reflect Fnx's complex star-formation history and potential merger events.
- N-rich field stars potential escapees from globular clusters (GCs) formed in dense environments — are absent in Dra, Car or Sex, consistent with their lack of GC as low-mass dwarfs. However, N-rich field stars were identified in Fnx. These stars exhibit no anomalous abundances in other measured elements and show metallicities distinct from known Fnx GCs, suggesting they may represent remnants of one or more dissolved GCs.

In the coming years, next-generation astronomical facilities such as the Extremely Large Telescope (ELT) and multi-fiber spectroscopic surveys (e.g., 4MOST, WEAVE, DESI) — will deliver increasingly detailed chemical profiles of member stars within dwarf galaxies. These advancements will enable tighter constraints on abundance patterns at the metal-poor end, a critical input for modeling the early evolutionary stages of these systems. By conducting comprehensive studies of dwarf galaxies across a range of mass scales, we will gain transformative insights into their formation histories and dynamical interactions, significantly advancing our understanding of galaxy evolution and the cosmic processes shaping these faint stellar systems.

Acknowledgements. C.X. and B.T. gratefully acknowledge support from the National Natural Science Foundation of China through grants NOs. 12233013 and 12473035, China Manned Space Project under grant NO. CMS-CSST-2025-A13 and CMS-CSST-2021-A08, the Fundamental Research Funds for the Central Universities, Sun Yat-sen University (24qnpy121). J.G.F.-T. gratefully acknowledges the grant support provided by ANID Fondecyt Iniciación No. 11220340, ANID Fondecyt Postdoc No. 3230001, and from the Joint Committee ESO-Government of Chile under the agreement 2023 ORP 062/2023. Z.Y. acknowledges the support from the National Natural Science Foundation of China under grant numbers 12203021. D.G. gratefully acknowledges the support provided by Fondecyt regular no. 1220264. D.G. also acknowledges financial support from the Dirección de Investigación y Desarrollo de la Universidad de La Serena through the Programa de Incentivo a la Investigación de Académicos (PIA-DIDULS).

#### References

```
Abdurro'uf, Accetta, K., Aerts, C., et al. 2022, ApJS, 259, 35
Adamo, A., Bradley, L. D., Vanzella, E., et al. 2024, Nature, 632, 513
Allende Prieto, C., Beers, T. C., Wilhelm, R., et al. 2006, ApJ, 636, 804
Alonso, A., Arribas, S., & Martínez-Roger, C. 1999, A&AS, 140, 261
Alvarez, R. & Plez, B. 1998, A&A, 330, 1109
Amarsi, A. M., Lind, K., Osorio, Y., et al. 2020, A&A, 642, A62
Amorisco, N. C. & Evans, N. W. 2012, ApJ, 756, L2
Arnett, W. D. 1971, ApJ, 166, 153
```

Arnould, M., Goriely, S., & Jorissen, A. 1999, A&A, 347, 572

Asplund, M., Grevesse, N., & Sauval, A. J. 2005, in Astronomical Society of the Pacific Conference Series, Vol. 336, Cosmic Abundances as Records of Stellar Evolution and Nucleosynthesis, ed. I. Barnes, Thomas G. & F. N. Bash,

Barklem, P. S., Christlieb, N., Beers, T. C., et al. 2005, A&A, 439, 129 Bastian, N. & Lardo, C. 2018, ARA&A, 56, 83 Battaglia, G., Tolstoy, E., Helmi, A., et al. 2006, A&A, 459, 423 Beaton, R. L., Oelkers, R. J., Hayes, C. R., et al. 2021, AJ, 162, 302 Bell, E. F., McIntosh, D. H., Katz, N., & Weinberg, M. D. 2003, ApJS, 149, 289 Belokurov, V., Erkal, D., Evans, N. W., Koposov, S. E., & Deason, A. J. 2018, MNRAS, 478, 611

Bensby, T., Feltzing, S., & Oey, M. S. 2014, A&A, 562, A71 Bisterzo, S., Travaglio, C., Gallino, R., Wiescher, M., & Käppeler, F. 2014, ApJ,

Blanton, M. R., Bershady, M. A., Abolfathi, B., et al. 2017, AJ, 154, 28 Bowen, I. S. & Vaughan, A. H., J. 1973, Appl. Opt., 12, 1430 Busso, M., Gallino, R., Lambert, D. L., Travaglio, C., & Smith, V. V. 2001, ApJ,

Carlin, J. L., Sheffield, A. A., Cunha, K., & Smith, V. V. 2018, ApJ, 859, L10 Carretta, E., Bragaglia, A., Gratton, R. G., et al. 2010, A&A, 516, A55 Cayrel, R., Depagne, E., Spite, M., et al. 2004, A&A, 416, 1117 Chen, Y. & Gnedin, O. Y. 2023, MNRAS, 522, 5638 Côté, B., Fryer, C. L., Belczynski, K., et al. 2018, ApJ, 855, 99 de los Reyes, M. A. C., Kirby, E. N., Ji, A. P., & Nuñez, E. H. 2022, ApJ, 925, 66

Eisenstein, D. J., Weinberg, D. H., Agol, E., et al. 2011, AJ, 142, 72 Feltzing, S. & Feuillet, D. 2023, ApJ, 953, 143

Fernández-Trincado, J. G., Beers, T. C., Barbuy, B., et al. 2022, A&A, 663, A126 Fernández-Trincado, J. G., Beers, T. C., Minniti, D., et al. 2020, ApJ, 903, L17 Fernández-Trincado, J. G., Beers, T. C., Minniti, D., et al. 2021, A&A, 648, A70 Fernández-Trincado, J. G., Beers, T. C., Tang, B., et al. 2019, MNRAS, 488, 2864

Fernández-Trincado, J. G., Robin, A. C., Moreno, E., et al. 2016, ApJ, 833, 132 Fernández-Trincado, J. G., Zamora, O., García-Hernández, D. A., et al. 2017, ApJ, 846, L2

Forbes, D. A., Alabi, A., Romanowsky, A. J., Brodie, J. P., & Arimoto, N. 2020, MNRAS, 492, 4874

Foster, C., Hopkins, A. M., Gunawardhana, M., et al. 2012, A&A, 547, A79 Fulbright, J. P. 2000, AJ, 120, 1841

Gaia Collaboration, Helmi, A., van Leeuwen, F., et al. 2018, A&A, 616, A12 González Hernández, J. I. & Bonifacio, P. 2009, A&A, 497, 497

Grebel, E. K., Gallagher, III, J. S., & Harbeck, D. 2003, AJ, 125, 1926 Gustafsson, B., Edvardsson, B., Eriksson, K., et al. 2008, A&A, 486, 951

Hasselquist, S., Hayes, C. R., Lian, J., et al. 2021, ApJ, 923, 172 Hasselquist, S., Shetrone, M., Smith, V., et al. 2017, ApJ, 845, 162

Helmi, A., Babusiaux, C., Koppelman, H. H., et al. 2018, Nature, 563, 85 Hodge, P. 1989, ARA&A, 27, 139

Hodge, P. W. 1971, ARA&A, 9, 35

Horta, D., Schiavon, R. P., Mackereth, J. T., et al. 2021, MNRAS, 500, 1385 Huang, K.-W. & Koposov, S. E. 2021, MNRAS, 500, 986

Huang, R., Tang, B., Li, C., et al. 2024, Science China Physics, Mechanics, and Astronomy, 67, 259513

Ibata, R., Lewis, G. F., Martin, N. F., Bellazzini, M., & Correnti, M. 2013, ApJ, 765, L15

Karakas, A. I. & Lattanzio, J. C. 2014, PASA, 31, e030

Kirby, E. N., Gilbert, K. M., Escala, I., et al. 2020, AJ, 159, 46

Kobayashi, C., Karakas, A. I., & Lugaro, M. 2020, ApJ, 900, 179

Kobayashi, C., Umeda, H., Nomoto, K., Tominaga, N., & Ohkubo, T. 2006, ApJ,

Kowalczyk, K. & Łokas, E. L. 2022, A&A, 659, A119

Lagarde, N., Decressin, T., Charbonnel, C., et al. 2012, A&A, 543, A108

Larsen, S. S., Eitner, P., Magg, E., et al. 2022, A&A, 660, A88 Law, D. R. & Majewski, S. R. 2010, ApJ, 718, 1128

Lequeux, J., Peimbert, M., Rayo, J. F., Serrano, A., & Torres-Peimbert, S. 1979, A&A, 80, 155

Letarte, B., Hill, V., Jablonka, P., et al. 2006, A&A, 453, 547 Li, C., Tang, B., Milone, A. P., et al. 2021, ApJ, 906, 133 Li, H. & Gnedin, O. Y. 2019, MNRAS, 486, 4030 Limongi, M. & Chieffi, A. 2006, ApJ, 647, 483

```
Lind, K., Koposov, S. E., Battistini, C., et al. 2015, A&A, 575, L12
```

Magrini, L., Randich, S., Kordopatis, G., et al. 2017, A&A, 603, A2

Majewski, S. R., Schiavon, R. P., Frinchaboy, P. M., et al. 2017, AJ, 154, 94

Majewski, S. R., Skrutskie, M. F., Weinberg, M. D., & Ostheimer, J. C. 2003, ApJ, 599, 1082

Martell, S. L., Shetrone, M. D., Lucatello, S., et al. 2016, ApJ, 825, 146

Massari, D., Koppelman, H. H., & Helmi, A. 2019, A&A, 630, L4

Masseron, T., Merle, T., & Hawkins, K. 2016, BACCHUS: Brussels Automatic Code for Characterizing High accUracy Spectra, Astrophysics Source Code Library, record ascl:1605.004

Masseron, T., Osorio, Y., García-Hernández, D. A., et al. 2021, A&A, 647, A24 McConnachie, A. W. 2012, AJ, 144, 4

McWilliam, A., Wallerstein, G., & Mottini, M. 2013, ApJ, 778, 149

Mészáros, S., Martell, S. L., Shetrone, M., et al. 2015, AJ, 149, 153

Milone, A. P., Marino, A. F., Piotto, G., et al. 2015, ApJ, 808, 51

Muñoz, R. R., Côté, P., Santana, F. A., et al. 2018, ApJ, 860, 66

Myeong, G. C., Vasiliev, E., Iorio, G., Evans, N. W., & Belokurov, V. 2019, MNRAS, 488, 1235

Nidever, D. L., Bovy, J., Bird, J. C., et al. 2014, ApJ, 796, 38

Nidever, D. L., Hasselquist, S., Hayes, C. R., et al. 2020, ApJ, 895, 88

Nidever, D. L., Holtzman, J. A., Allende Prieto, C., et al. 2015, AJ, 150, 173

Nissen, P. E., Amarsi, A. M., Skúladóttir, Á., & Schuster, W. J. 2024, A&A, 682, A116

Osorio, Y., Allende Prieto, C., Hubeny, I., Mészáros, S., & Shetrone, M. 2020, A&A, 637, A80

Pace, A. B. 2024, arXiv e-prints, arXiv:2411.07424

Pace, A. B., Walker, M. G., Koposov, S. E., et al. 2021, ApJ, 923, 77

Pancino, E., Romano, D., Tang, B., et al. 2017, A&A, 601, A112

Plez, B. 2012, Turbospectrum: Code for spectral synthesis, Astrophysics Source Code Library, record ascl:1205.004

Reddy, B. E., Lambert, D. L., & Allende Prieto, C. 2006, MNRAS, 367, 1329 Reddy, B. E., Tomkin, J., Lambert, D. L., & Allende Prieto, C. 2003, MNRAS,

340, 304 Reichert, M., Hansen, C. J., Hanke, M., et al. 2020, A&A, 641, A127

Roederer, I. U., Preston, G. W., Thompson, I. B., et al. 2014, AJ, 147, 136

Sanders, J. L., Belokurov, V., & Man, K. T. F. 2021, MNRAS, 506, 4321

Santana, F. A., Beaton, R. L., Covey, K. R., et al. 2021, AJ, 162, 303

Schiavon, R. P., Zamora, O., Carrera, R., et al. 2017, MNRAS, 465, 501

Schlegel, D. J., Finkbeiner, D. P., & Davis, M. 1998, ApJ, 500, 525

Shetrone, M., Venn, K. A., Tolstoy, E., et al. 2003, AJ, 125, 684

Simon, J. D. 2019, ARA&A, 57, 375

Smith, V. V., Cunha, K., Shetrone, M. D., et al. 2013, ApJ, 765, 16

Tang, B., Cohen, R. E., Geisler, D., et al. 2017, MNRAS, 465, 19

Tang, B., Fernández-Trincado, J. G., Geisler, D., et al. 2018, ApJ, 855, 38

Tang, B., Fernández-Trincado, J. G., Liu, C., et al. 2020, ApJ, 891, 28

Tang, B., Liu, C., Fernández-Trincado, J. G., et al. 2019, ApJ, 871, 58

Tang, B., Wang, Y., Huang, R., et al. 2021, ApJ, 908, 220 Tang, B., Zhang, J., Yan, Z., et al. 2023, A&A, 669, A125

Tinsley, B. M. 1979, ApJ, 229, 1046

Tolstoy, E., Hill, V., & Tosi, M. 2009, ARA&A, 47, 371

Walker, M. G. & Peñarrubia, J. 2011, ApJ, 742, 20

Wang, M. Y., Koposov, S., Drlica-Wagner, A., et al. 2019, ApJ, 875, L13

Watson, D., Hansen, C. J., Selsing, J., et al. 2019, Nature, 574, 497

Weinberg, D. H., Holtzman, J. A., Hasselquist, S., et al. 2019, ApJ, 874, 102

Weisz, D. R., Dolphin, A. E., Skillman, E. D., et al. 2014, ApJ, 789, 147

Woosley, S. E. & Weaver, T. A. 1995, ApJS, 101, 181

Woosley, S. E., Wilson, J. R., Mathews, G. J., Hoffman, R. D., & Meyer, B. S. 1994, ApJ, 433, 229

Yong, D., Norris, J. E., Bessell, M. S., et al. 2013, ApJ, 762, 27

Yu, J., Tang, B., Fernández-Trincado, J. G., et al. 2021, ApJ, 913, 23

Zamora, O., García-Hernández, D. A., Allende Prieto, C., et al. 2015, AJ, 149, 181

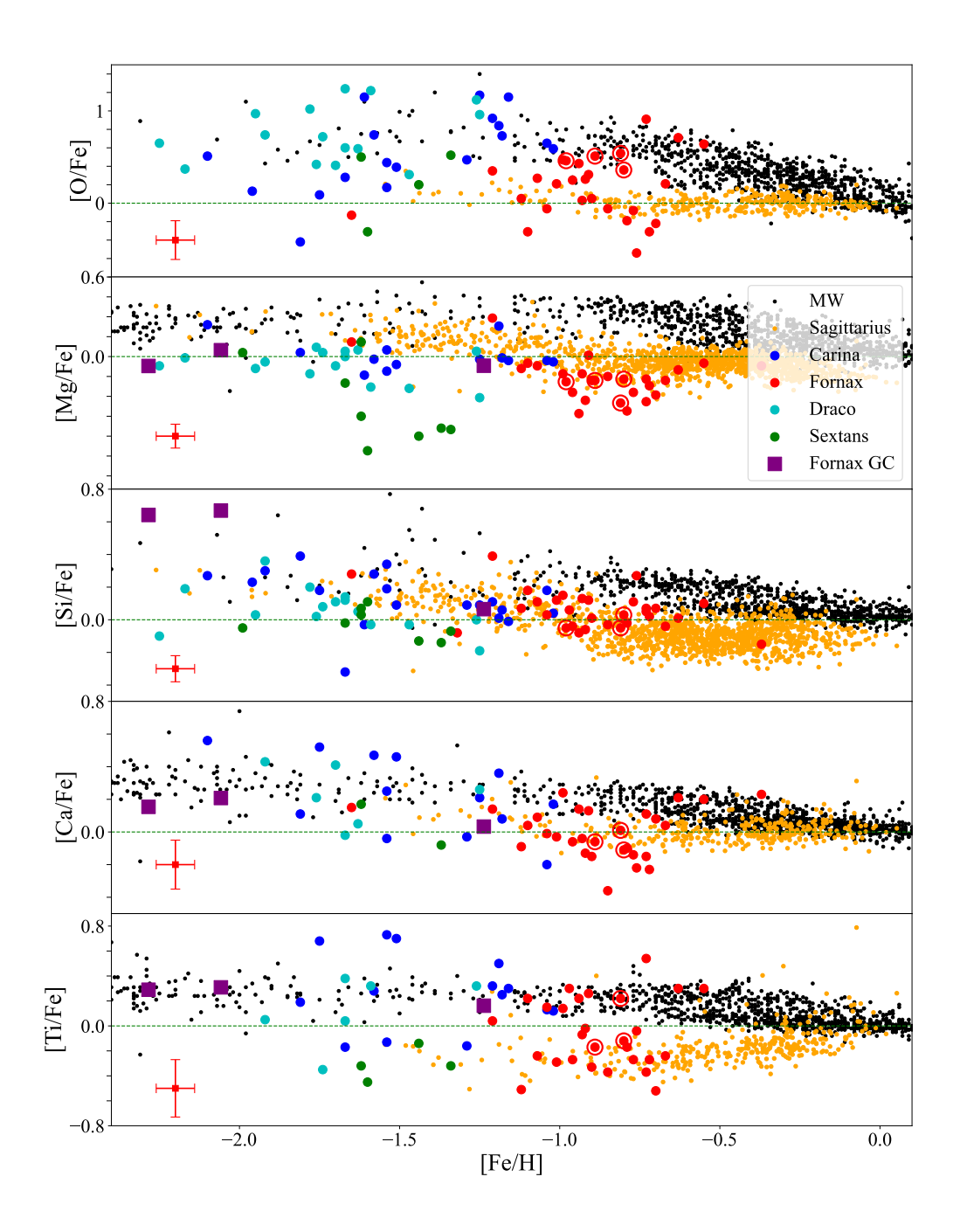
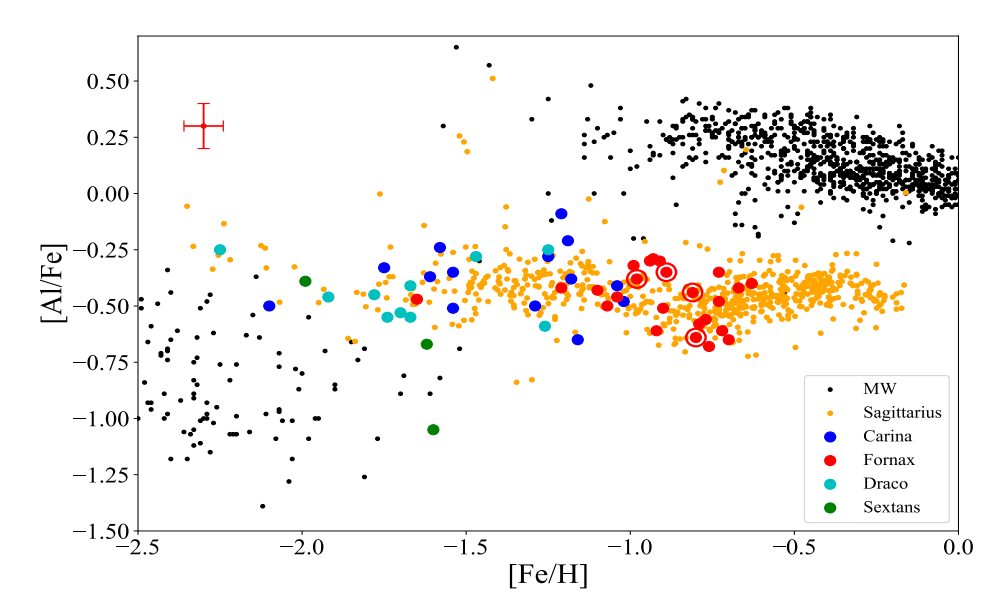
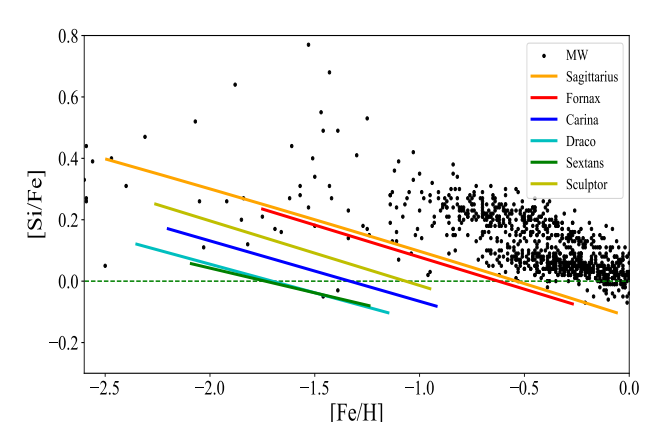


Fig. 2. [ $\alpha$ /Fe] vs. [Fe/H]. Fnx, Dra, Car and Sex stars from this work are labeled as red, cyan, blue and green stars respectively. The error bar in each panel indicates the median uncertainty of available measurements. Black dots correspond to MW stars from the halo (Fulbright 2000; Cayrel et al. 2004; Barklem et al. 2005; Yong et al. 2013; Roederer et al. 2014), and MW stars from the disc (Reddy et al. 2003, 2006; Bensby et al. 2014). Orange dots represent Sgr stars from Hasselquist et al. (2021). Purple squares represent GCs in Fnx from Larsen et al. (2022)



 $\textbf{Fig. 3.} \ [\text{Al/Fe}] \ \text{vs.} \ [\text{Fe/H}] \ \text{relations.} \ \text{Symbols are the same as in Fig. 2}.$ 



**Fig. 4.** Derived LTE abundances of [Si/Fe] over metallicities for individual dwarf galaxies. MW stars (black dots) are described in Fig. 2. The best polynomial fits to the data of Sgr, Fnx, Dra, Car, Sex and Scl member stars are labeled as orange, red, cyan, blue, green, and yellow lines.

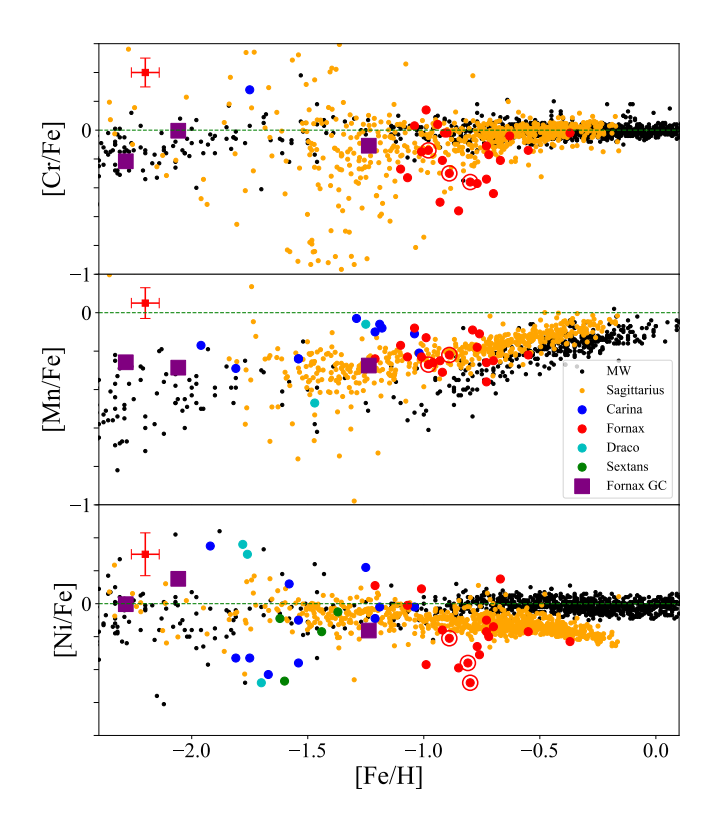


Fig. 5. Abundances of iron peak elements vs. [Fe/H]. Symbols are the same as in Fig. 2.

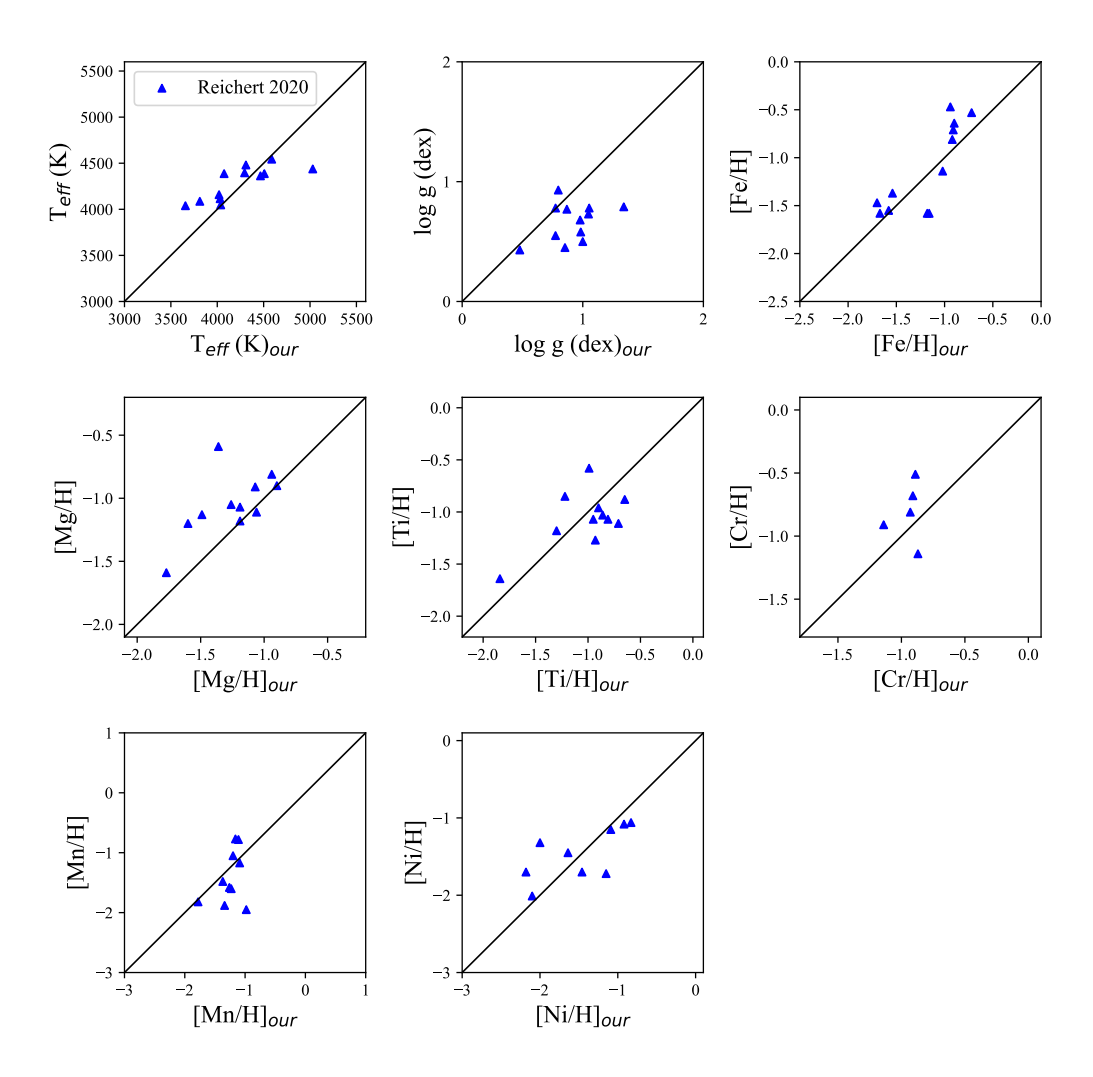
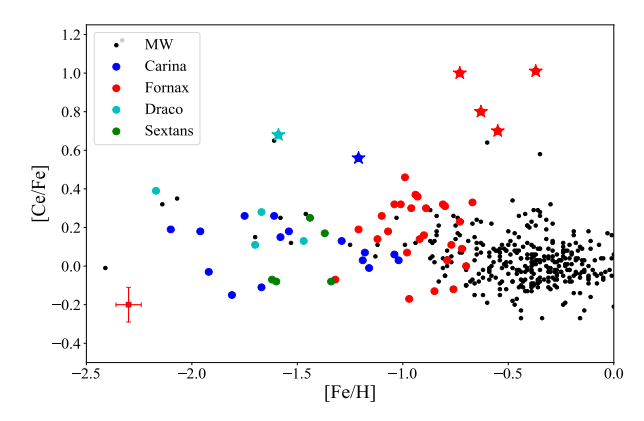
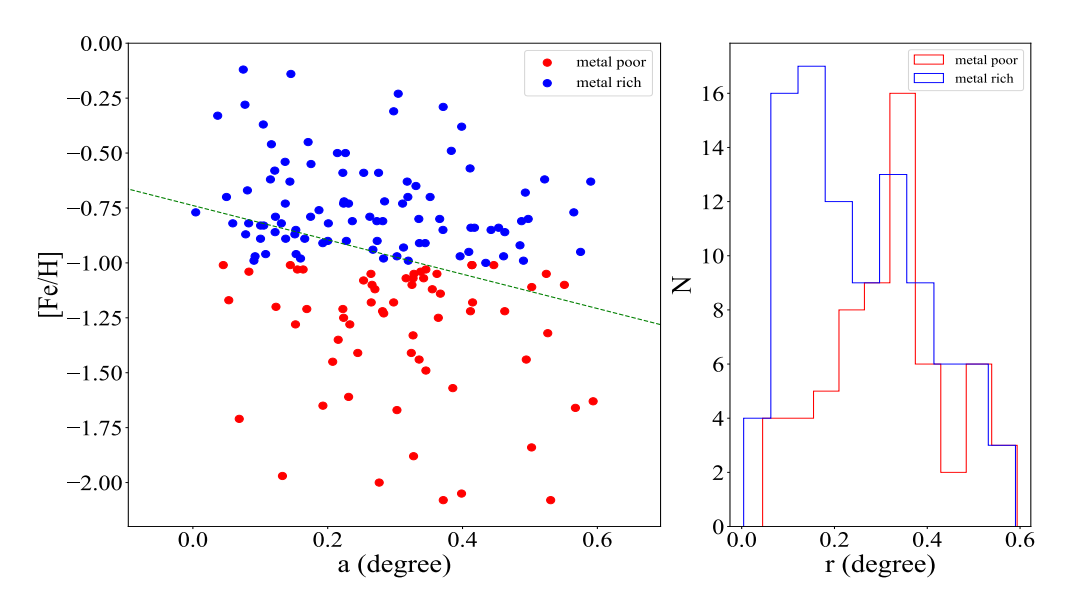


Fig. 6. Comparison of stellar parameters and chemical abundances of this work with those from the R20. Our results are denoted "our" and shown in the x-axis. The black solid line is the 1:1 relation.



**Fig. 7.** [Ce/Fe] vs. [Fe/H]. Symbols are the same as in Fig. 2. Notably, the stars marked with star symbols are those with [Ce/Fe] greater than 0.5, which are likely AGB stars.



**Fig. 8.** Metallicity distribution of stars in Fnx. Left panel: [Fe/H] as a function of elliptical radius in degrees. The green dashed line represents the best least-squared fit. They are divided into a metal-rich population ([Fe/H] > -1, blue dots) and a metal-poor population ([Fe/H] < -1, red dots). Right panel: the radial distribution of the metal-rich population (blue histogram) and the metal-poor population (red histogram).

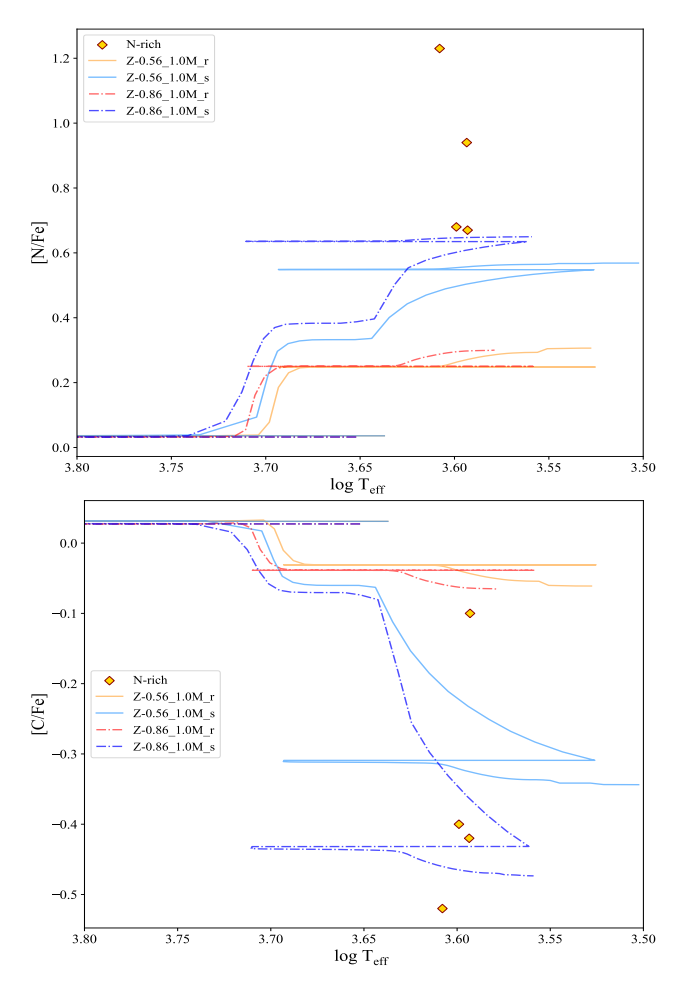


Fig. 9. Abundance comparison between our identified N-rich stars (gold diamonds) and Lagarde2012 model predictions. Blue and orange lines represent model predictions for the stellar mass of 1.0  $M_{\odot}$  in the primordial and mixing-enriched stellar populations, while solid and dashed lines represent those for [Fe/H] = -0.86 and -0.56, respectively.

# Appendix A: Information on all sample stars

Table A.1. Basic information on all sample stars

Table   Tabl			D.1	P.F.G							
1 2M02403081.3422028	#	APOGEE ID	RA	DEC [deg]	T <sub>eff</sub>	$\log g$	<i>RV</i> [km s <sup>-1</sup> ]	S/N	Gmag	BP-RP	Dwarf Galaxy
2 2M002372118-3437451			[ueg]	[ueg]	[K]		[KIII 8 ]		[mag]	[mag]	_
3 2M02392578-3442220 39.85744 - 34.70617 3886 0.27 59 130 17.40 2.19 Fnx 4 2M02402543-415209 40.09813 - 34.25565 3552 0.24 36 96 17.70 2.06 Fnx 5 2M02413913-3405509 40.09813 - 34.25565 3552 0.24 36 96 17.70 2.06 Fnx 7 2M02410066-3415551 40.52077 - 34.26532 3960 6.05 54 114 17.51 2.18 Fnx 8 2M02336004-34449] 39.59015 - 344.3009 39.0015 - 34.2590 39.5015 - 34.2590 39.5015 - 34.2590 39.5015 - 34.2590 39.5015 - 34.2590 39.5015 - 34.2590 39.5015 - 34.2590 39.5015 - 34.2590 39.5015 - 34.2590 39.5015 - 34.2590 39.5015 - 34.2590 39.5015 - 34.54732 40.54 1.01 57 76 17.85 1.83 Fnx 11 2M02373820-3424530 39.9018 - 34.41473 3668 0.48 65 84 17.64 1.92 Fnx 12 2M02373820-3445302 39.88889 - 34.66104 4037 1.00 42 70 17.89 1.77 Fnx 14 2M0238595-3446302 39.4808 - 34.78179 4019 0.98 31 71 17.88 1.77 Fnx 15 2M02375883-3447160 39.48286 - 34.78179 4019 0.98 31 71 17.88 1.77 Fnx 16 2M02373820-3432530 39.58516 - 34.58180 3918 0.79 41 106 17.49 1.99 Fnx 18 2M02392383-3432530 39.56201 - 34.58187 3922 0.89 55 101 17.63 2.13 Fnx 18 2M0239397-3341553 39.87012 - 34.58985 3972 0.96 5 4 71 17.87 1.86 Fnx 18 2M0239393820-3445030 39.6200 - 34.51817 3922 0.89 55 101 17.63 2.13 Fnx 2M02393983-3419234 39.8829 - 34.34388 39.72355 - 34.58985 39.59 5 5 101 17.63 2.13 Fnx 2M02393983-3419234 39.88249 - 34.38385 39.7355 - 54.5184 39.87812 0.77 5 61 17.69 1.78 1.86 Fnx 2M02393198-3419234 39.88249 - 34.38385 39.7355 - 54.5184 39.87812 0.79 17.85 1.86 Fnx 2M02393198-3419234 39.88249 - 34.38385 39.50 5 5 7 10 17.65 1.66 Fnx 2M02393198-3419234 39.88269 - 34.34380 39.8829 - 34.32318 3495 0.65 5 4 71 17.87 1.86 Fnx 2M02393198-3419234 39.88269 - 34.32318 3495 0.65 5 4 71 17.87 1.86 Fnx 2M02393198-3419234 39.88269 - 34.32318 3495 0.65 5 4 71 17.87 1.86 Fnx 2M02393198-3419234 39.88670 - 34.38385 39.50 0.65 5 4 71 17.87 1.86 Fnx 2M0240239385-3419234 39.88690 - 34.36363 - 34.36794 30.99 1.79 1.79 1.79 1.79 1.79 1.79 1.79 1											
4 2M02402354-3415204 40,09813 -34,25565 3552 0.24 36 96 17.70 2.06 Fnx 5 2M00241913-3340555 40,41308 -34,0736 3684 0.56 59 78 17.84 1.82 Fnx 6 2M02381712-3425482 39,57135 -34,43009 3696 0.56 54 114 17.51 2.18 Fnx 7 2M024006-3415551 40,25277 -34,26532 3796 0.72 57 80 17.78 1.86 Fnx 8 2M02380004-3444219 9,950015 -34,73947 3806 0.75 40 84 17.80 1.88 Fnx 9 2M02372718-3430033 39,36329 -34,50905 4012 0.97 50 72 17.86 1.79 Fnx 10 2M02390557-3432503 39,07332 -34,54732 4054 1.01 57 76 17.85 1.83 Fnx 11 2M02373820-3424530 39,40918 -34,4173 3806 0.49 53 96 17.56 2.00 Fnx 12 2M0239333-3438302 39,8889 -34,64173 3800 0.69 53 96 17.56 2.00 Fnx 13 2M02384789-343997 39,4826 -34,78779 4019 0.98 31 71 17.89 1.77 Fnx 14 2M02385365-3434048 39,67352 -34,55104 4031 0.85 31 71 17.88 1.77 Fnx 15 2M02375588-3447160 39,67132 -34,73905 4031 0.85 50 70 17.61 1.64 Fnx 17 2M02385365-3431034 39,8236 -34,78779 4019 0.98 31 71 17.85 1.87 Fnx 18 2M02392348-3432530 39,85161 -34,55134 3812 0.77 39 77 17.85 1.87 Fnx 18 2M0239237807-3431053 39,62601 -34,75087 3565 0.24 56 86 17.66 1.95 Fnx 2 2M02393076-3451354 39,87812 -34,85985 3972 0.96 54 71 17.87 1.86 Fnx 2 2M02393076-3451354 39,87812 -34,85985 3972 0.96 54 71 17.87 1.86 Fnx 2 2M02393076-3451354 39,887812 -34,85985 3972 0.96 54 71 17.87 1.86 Fnx 2 2M0239308-3432342 39,27432 -34,5286 3733 0.61 46 85 17.69 1.91 Fnx 2 2M0239308-342521 39,92432 -34,5286 3733 0.61 46 85 17.69 1.91 Fnx 2 2M0239308-342521 39,92432 -34,5286 3733 0.61 46 85 17.69 1.91 Fnx 2 2M0239308-342521 39,92432 -34,5286 3733 0.61 46 85 17.69 1.91 Fnx 18.2 Fnx 2 2M0239308-342531 39,8870 -34,24493 30,8830 -34,3030 -34,3											
5         2M02413913-3405505         40.41308         -34.400736         3684         0.56         59         78         17.84         1.82         Finx           6         2M02310066-3415551         -34.43003         3666         0.56         54         114         17.51         2.18         Finx           7         2M02410066-3415551         9         2M02372718-343003         39.56329         -34.73947         3806         0.75         40         84         17.80         1.88         Finx           9         2M02372718-343003         39.36329         -34.50095         4012         0.97         50         72         17.86         1.79         Finx           10         2M0237333-3438002         39.47918         -34.44733         3668         0.48         65         84         17.66         2.00         Finx           12         2M0237333-348302         39.74808         -34.46103         30.00         6.08         33         61         7.56         2.00         Finx           12         2M0233418-344205         39.48368         -34.76010         3779         0.72         23.3         0.17.56         2.00         Finx           18         2M023348113-3444205         39.76132<											
6 2M02381712-3425482 39.57135 -34.43009 3696 0.56 54 114 17.51 2.18 Fnx 7 2M0214006-3415513 40.25277 -34.26532 3796 0.72 57 80 17.78 1.86 Fnx 8 2M02380004.344219 9.50015 -34.73947 3806 0.75 40 84 17.30 1.88 Fnx 9 2M02372718-3430033 39.6329 -34.5009 4012 0.97 50 72 17.86 1.79 Fnx 10 2M02390557-3432503 39.73723 -34.54732 4054 1.01 57 76 17.85 1.83 Fnx 11 2M02373820-3424530 39.40918 -34.41473 3668 0.48 65 84 17.64 1.92 Fnx 12 2M0239333-348302 39.8889 -34.64173 3800 0.69 53 96 17.56 2.00 Fnx 13 2M02384789-3439397 39.8889 -34.64173 3800 0.69 53 96 17.56 2.00 Fnx 14 2M023358365-343408 39.78486 -34.78779 4019 0.98 31 71 17.89 1.77 Fnx 15 2M02375588-3447160 39.67856 -34.56104 4037 1.00 42 70 17.89 1.77 Fnx 15 2M02375588-3447160 39.67856 -34.56104 4037 1.00 42 70 17.89 1.77 Fnx 15 2M02375588-3447160 39.67132 -34.73905 4031 0.85 50 70 17.61 1.64 Fnx 17 2M02383365-3433048 39.272355 -34.55134 3812 0.77 39 77 17.85 1.87 Fnx 18 2M02392438-3432530 39.85161 -34.55810 3918 0.79 41 106 17.49 1.99 Fnx 19 2M02383024-3445030 39.62601 -34.75087 3918 3918 0.79 41 106 17.49 1.99 Fnx 2M02393076-3451354 39.87812 -34.58935 3972 0.96 54 71 17.87 1.86 Fnx 18 2M02393108-3432342 39.87812 -34.85985 3972 0.96 54 71 17.87 1.86 Fnx 2M02393108-3419234 39.88329 -34.2318 3495 0.65 54 71 17.87 1.86 Fnx 2M02393198-3419234 39.88329 -34.2318 3495 0.65 54 71 17.87 1.86 Fnx 2M02393198-3419234 39.88329 -34.2318 3495 0.65 54 71 17.87 1.86 Fnx 2M02393198-3419234 39.88329 -34.2318 3495 0.65 54 71 17.87 1.86 Fnx 2M02393198-3419231 39.6784 -34.54036 657 0.48 40 84 17.77 1.82 Fnx 2M02393198-341931 39.88329 -34.2318 3495 0.65 54 71 17.87 1.86 Fnx 31 2M02393198-341931 39.88329 -34.2318 3495 0.65 54 71 17.87 1.86 Fnx 31 2M02393198-341931 39.88329 -34.2318 3495 0.65 54 71 17.83 1.82 Fnx 31 2M02393198-341931 39.88461 -34.20371 3747 0.63 45 82 17.70 1.89 Fnx 31 2M02393038-3431934 39.88329 -34.2318 3495 0.65 54 71 17.83 1.82 Fnx 31 2M023930393285-341709 39.8950 39.8860 39.8860 39.8860 39.9860 39.8760 39.9860 39.8760 39.9860 39.8760 39.9860 39.8760 39.9860 39.8760 39.9											
7 2M02410066-3415S51											
8 2M02380004-3444219 39.50015 -34.73947 806 0.75 40 84 17.80 1.88 Fnx   9 2M02372718-3430333 39.50239 -34.50095 4012 0.97 50 72 17.86 1.79 Fnx   10 2M02390357-3432503 39.77323 -34.54732 40.54 1.01 57 76 17.85 1.83 Fnx   11 2M0239333-3438302 39.88889 -34.64173 3800 0.69 53 96 17.56 2.00 Fnx   12 2M0239333-3438302 39.88889 -34.64173 3800 0.69 53 96 17.56 2.00 Fnx   13 2M02384789-3439397 39.59955 -34.66104 4037 1.00 42 70 17.89 1.77 Fnx   14 2M02355854-3447362 39.74808 -34.78779 40.19 0.98 31 71 17.88 1.77 Fnx   15 2M02375588-3447160 39.48286 -34.78779 40.19 0.98 31 71 17.88 1.77 Fnx   16 2M02385365-3433048 39.72355 -34.5134 3812 0.77 39 77 17.85 1.87 Fnx   17 2M02385365-3433048 39.72355 -34.55134 3812 0.77 39 77 17.85 1.87 Fnx   18 2M02392438-3432533 39.8516 1 -34.54810 3918 0.79 41 10.6 17.49 1.99 Fnx   19 2M02383024-3445030 39.62601 -34.475087 3565 0.24 56 86 17.66 1.95 Fnx   22 2M02393106-3451354 39.8702 -34.51817 3922 0.89 55 101 17.63 2.13 Fnx   22 2M02394140-3422511 39.92243 -34.38085 3715 0.64 59 72 17.87 1.86 Fnx   23 2M02393108-3432342 39.27432 -34.485085 3715 0.64 59 72 17.87 1.86 Fnx   24 2M02393198-3419234 39.88329 -34.32318 395 0.65 54 71 17.83 1.82 Fnx   24 2M02393198-3419234 39.88329 -34.32318 395 0.65 54 71 17.83 1.82 Fnx   25 2M023923285-3417023 39.88670 -34.28409 4126 1.70 56 101 17.57 2.21 Fnx   26 2M02392221-3412133 39.84261 -34.20371 3747 0.63 45 82 17.70 1.89 Fnx   27 2M023934018-343912 39.66743 -34.20371 3747 0.63 45 82 17.70 1.89 Fnx   28 2M02412486-3422044 40.53503 -34.20371 3747 0.63 45 82 17.70 1.89 Fnx   28 2M02412486-3422044 40.53503 -34.20371 3747 0.63 45 82 17.70 1.89 Fnx   28 2M02412486-3422044 39.991870 -34.20371 3747 0.63 45 82 17.70 1.89 Fnx   32 2M0239306-342419 39.991870 -34.20371 3747 0.63 45 82 17.70 1.89 Fnx   32 2M0239306-342419 39.991870 -34.20371 3747 0.63 45 82 17.70 1.89 Fnx   32 2M0239306-342419 39.991870 -34.20371 3747 0.63 45 82 17.70 1.89 Fnx   32 2M02412486-3422044 40.55363 -34.6064 40.0064 40.0064 40.0064 40.0064 40.0064 40.0064 40.0064 40.0064 40.0064 40.0064 40											
9 2M023727I8-3430033 39.36329 -34.50095 4012 0.97 50 72 17.86 17.9 Fnx 10 2M02373820-3424530 39.7323 -34.54732 4054 1.01 57 76 17.85 1.83 Fnx 11 2M02373820-3424530 39.40918 -34.41473 3668 0.48 65 84 17.64 1.92 Fnx 12 2M0233333-3438302 39.88889 -34.64173 3800 0.69 53 96 17.56 2.00 Fnx 13 2M02384789-3439397 39.69955 -34.66104 4037 1.00 42 70 17.88 1.77 Fnx 14 2M02385954-3445362 39.74808 -34.76010 3779 0.72 53 70 17.85 1.83 Fnx 15 2M02375588-3447160 39.48286 -34.78779 4019 0.98 31 71 17.88 1.87 Fnx 16 2M02384113-3444205 39.67132 -34.73905 4031 0.85 50 70 17.61 1.64 Fnx 17 2M02384313-3444205 39.67132 -34.54810 3918 0.77 39 77 17.85 1.87 Fnx 18 2M02392438-342530 39.85161 -34.54810 3918 0.79 41 106 17.49 1.99 Fnx 19 2M02383024-344503 39.2601 -34.75087 3565 0.24 56 86 17.66 1.95 Fnx 22 2M02392076-3451354 39.378312 -34.54810 3918 0.79 41 106 17.49 1.99 Fnx 22 2M02393076-3451354 39.378312 -34.54810 3918 0.79 41 106 17.49 1.99 Fnx 22 2M02393076-3451354 39.878312 -34.54866 3733 0.61 46 85 17.69 1.95 Fnx 23 2M02370583-3432342 39.878312 -34.54866 3733 0.61 46 85 17.69 1.91 Fnx 24 2M0239308-3449234 39.88329 -34.52318 3495 0.65 54 71 17.87 1.86 Fnx 25 2M02392385-3417028 39.88670 -34.28409 1.426 1.70 56 101 17.57 2.21 Fnx 27 2M02384018-3439121 39.66743 -34.63363 657 0.48 40 84 17.77 1.82 Fnx 28 2M02412486-3422044 39.88329 -34.42318 3495 0.65 54 71 17.88 1.82 Fnx 28 2M02412486-3422044 30.35363 -34.36794 370 0.55 6 101 17.57 2.21 Fnx 29 2M02393861-3425279 39.99427 -34.42443 3020 0.32 57 140 17.24 2.30 Fnx 31 2M02393365-3422049 39.91870 -34.20702 415 1.11 45 75 17.82 1.76 Fnx 32 2M02393861-3425279 39.99427 -34.42443 3020 0.32 57 140 17.24 2.30 Fnx 32 2M17193604-5756289 259.9003 57.98609 4883 1.03 -229 79 85 17.03 1.59 Pnx 32 2M1719342-57558082577 29.98019 58.00726 4888 1.06 -292 107 16.79 1.56 Dna 32 2M1719342-5753605 20.55663 57.98564 4209 0.66 -289 101 16.80 1.99 Pnx 32 2M1719342-5753648 259.99080 57.99659 4399 0.89 -293 72 17.10 1.47 Dna 42 2M1719134-5759007 20.06658 37.88561 4209 0.89 -293 72 17.10 1.47 Dna 42 2M1719476-75748											
10   2M02390557-3432503   39,47032   3-45,4732   4054   1.01   57   76   17.85   1.83   Fnx   12M023873820-3424530   39,470818   -34,461473   3668   0.48   65   84   17.64   1.92   Fnx   13   2M0238739-3439397   39,69955   -34,66104   3077   1.00   42   70   17.89   1.77   Fnx   1.78   1.77   Fnx   1.78   2M02375588-3447160   39,48286   -34,78779   4019   0.98   31   71   17.88   1.77   Fnx   1.78   2M02385365-3433048   39,48286   -34,78779   4019   0.98   31   71   17.88   1.77   Fnx   1.78   2M02385365-3433048   39,72355   -34,5134   3812   0.77   39   77   17.85   1.87   Fnx   2M02385365-3433048   39,72355   -34,5134   3812   0.77   39   77   17.85   1.87   Fnx   2M02383024-3445030   39,62601   -34,75087   3665   0.24   56   86   17.66   1.95   Fnx   1.2   2M0239076-3451354   39,87812   -34,51387   39,2243   39,37812   -34,51387   39,2243   39,37812   -34,51387   39,2243   39,37812   34,51384   34,51384   39,37812   34,51384   39,37812   34,51384   39,37812   34,51384   39,37812   34,51384   39,37812   34,51384   39,37812   34,51384   39,37812   34,51384   39,37812   34,51384   39,37812   34,51384   39,37812   34,51384   39,37812   34,51384   39,37812   34,51384   39,37812   34,51384   39,37812   34,51384   39,37812   34,51384   39,37812   34,51384   39,37812   34,51384											
11   2M02373820-3424530   39.40918   -34.41473   3668   0.48   6.5   8.4   17.64   1.92   Firx   2M023895333-3438302   39.88889   -34.61713   3800   0.69   5.3   96   17.56   2.00   Firx   2M02384789-34435362   39.74808   -34.76010   377   0.72   5.3   70   17.85   1.83   Firx   7.8   1.82   Firx   2M02375588-3447160   39.48286   -34.78797   4019   0.98   31   71   17.88   1.77   Firx   1.72   2M02384113-3444205   39.67132   -34.73905   4031   0.85   50   70   17.61   1.64   Firx   2M023895365-3433048   39.72355   -34.55143   3812   0.77   39   77   17.85   1.83   1.87   Firx   1.8   2M02392438-3432530   39.85161   -34.54810   39.18   0.79   41   106   17.49   1.99   Firx   2M02392438-3432530   39.36702   -34.51817   39.22   0.89   5.5   101   17.63   2.13   Firx   2.2   2.											
12   2M02393333-3438302   39.88889   -34.64173   3800   0.69   53   96   17.56   2.00   Finx   2M023853653434793   39.6955   -34.66104   4037   1.00   42   70   17.85   1.83   Finx   1.77   Finx   1.20   2M02375588 3447160   39.48286   -34.78779   4019   0.98   31   71   17.88   1.77   Finx   1.77   Finx   1.20   2M02375588 3447160   39.48286   -34.78779   4019   0.98   31   71   17.88   1.77   Finx   1.20   2M02385365.3433048   39.48286   -34.58134   3812   0.77   39   77   17.85   1.87   Finx   1.20   2M02385365.3433048   39.72355   -34.55134   3812   0.77   39   77   17.85   1.87   Finx   1.20   2M023392438-3432530   39.85161   -34.54818   3918   0.79   41   106   17.49   1.99   Finx   1.20   2M02339076.3431353   39.6702   -34.51817   3922   0.89   55   101   17.63   2.13   Finx   2.20   2M023793763-3431354   39.87812   -34.85985   3972   0.96   54   71   17.87   1.86   Finx   2.20   2.2											
13   2M02384789-3439397   39.69955   -34.66104   4037   1.00   42   70   17.89   1.77   Finx   4002375588-3447160   39.48286   -34.78779   4019   0.98   31   71   17.85   1.83   Finx   4002375588-3447160   39.48286   -34.78779   4019   0.98   31   71   17.85   1.83   Finx   4002375588-3447160   39.48286   -34.78779   4019   0.98   31   71   17.85   1.87   Finx   4002384115-3444205   39.67152   -34.73905   4031   0.85   50   70   17.61   1.64   Finx   403234243   40323525   -34.55134   3812   0.77   39   77   17.85   1.87   Finx   4032392438-3432530   39.85161   -34.54810   3918   0.79   41   106   17.49   1.99   Finx   403233802-34454303   39.62601   -34.75087   3565   0.24   56   86   17.66   1.95   Finx   4032392387-3431053   39.36702   -34.51817   3922   0.89   55   101   17.63   2.13   Finx   4032392394140-3422511   39.92243   -34.85985   3972   0.96   54   71   17.87   1.86   Finx   4032392394140-3422511   39.9243   -34.85985   3972   0.96   54   71   17.87   1.86   Finx   4032393285-3417028   39.87812   -34.54286   3733   0.61   46   85   17.69   1.91   Finx   403239221-3412133   39.84261   -34.20371   3747   0.63   45   82   17.70   1.89   Finx   403239221-3412133   39.84261   -34.20371   3747   0.63   45   82   17.70   1.89   Finx   403239221-3412133   39.84261   -34.20371   3747   0.63   45   82   17.70   1.89   Finx   403239234949-3412351   40.1589   -34.20371   3747   0.63   45   82   17.70   1.89   Finx   4002393258-342419   39.89019   -34.41165   4519   1.37   42   70   17.86   1.89   Finx   4002393258-342419   39.89019   -34.41165   4519   1.37   42   70   17.86   1.89   Finx   4002393245815384   20023923   83.80602   4961   1.06   -274   107   16.71   1.54   Dra   42   42012783412351   40.11589   -34.20072   4215   1.11   45   75   17.84   1.87   Finx   400239365-3424419   39.89019   -34.41165   4519   1.37   42   70   17.86   1.89   Finx   400239365-3424419   39.89019   -34.41165   4519   1.37   42   70   17.86   1.89   Finx   400239365-3424419   39.89019   -34.41165   4519   1.37   42   70											
14   2M02385954.3445362   39.74808   -34.78719   4019   0.98   31   71   17.88   1.83   Finx     15   2M02385365.3434048   39.6261   -34.73905   4031   0.85   50   70   17.61   1.64   Finx     17   2M02385365.3433048   39.72355   -34.55143   3812   0.77   39   77   17.85   1.87   Finx     18   2M02383024.34342530   39.85161   -34.54810   3918   0.79   41   106   17.69   1.99   Finx     19   2M02383024.34443030   39.62601   -34.75187   3565   0.24   56   86   17.66   1.95   Finx     19   2M02383024.34443030   39.62601   -34.75187   3565   0.24   56   86   17.66   1.95   Finx     20   2M02372807.3431033   39.8702   -34.51134   391817   3922   0.89   55   101   17.63   2.13   Finx     21   2M02393076-3451354   39.87812   -34.85985   3972   0.96   54   71   17.87   1.86   Finx     22   2M02394140.3422511   39.92243   -34.54286   3733   0.61   46   85   17.69   1.91   Finx     24   2M02393198.3419234   39.88329   -34.32818   3495   0.65   54   71   17.83   1.82   Finx     25   2M02393285-3417028   39.88670   -34.28499   4126   1.70   56   101   17.57   2.21   Finx     26   2M02393285-3419121   39.66743   -34.63636   3657   0.48   40   84   17.77   1.82   Finx     27   2M02395861.3425279   39.99427   -34.42443   3620   0.52   57   140   17.24   2.30   Finx     29   2M02395863.442251   40.11580   -34.32071   3747   0.63   45   82   17.70   1.89   Finx     29   2M02395861.3425279   39.99427   -34.42443   3620   0.52   57   140   17.24   2.30   Finx     20   2M02394049.3419391   39.91870   -34.32756   4182   1.13   51   75   17.84   1.87   Finx     21   2M02394049.3419391   39.91870   -34.32756   4182   1.13   51   75   17.84   1.87   Finx     22   2M0239365.3424449   39.8910   -34.41165   51.9   1.37   42   70   1.67   1.54   Dra     24   2M17193600+5756289   259.90003   57.94136   4810   1.14   -289   31   17.13   1.48   Dra     24   24   24   24   24   24   38   38   38   38   38   39   -28   39   37   31   31   31   48   Dra     24   24   24   24   34   34   34   34											
15   2M02375588-3447160   39.48286   -34.78779   4019   0.98   31   71   17.88   1.77   Fnx   16   2M02385365-3433048   39.67132   -34.73905   4031   0.85   50   70   17.61   1.64   Fnx   17   2M02385365-3433048   39.72355   -34.55134   3812   0.77   39   77   17.85   1.87   Fnx   18   2M02392438-3432530   39.85161   -34.54810   3918   0.79   41   106   17.49   1.99   Fnx   18   2M02393026-34345030   39.65061   -34.75087   3565   0.24   56   86   17.66   1.95   Fnx   18   2M02392076-3431053   39.36702   -34.51817   3922   0.89   55   101   17.63   2.13   Fnx   2   2M02393076-3451354   39.87812   -34.85985   3972   0.96   54   71   17.87   1.86   Fnx   2   2M02394140-3422511   39.92243   -34.85985   3972   0.96   54   71   17.87   1.86   Fnx   2   2M02393198-349234   39.8329   -34.32318   3495   0.65   54   71   17.83   1.82   Fnx   2   2M02393198-349234   39.88529   -34.32318   3495   0.65   54   71   17.83   1.82   Fnx   2   2   2   2   2   2   2   2   2											
16   2M02384113-3444205   39.67132   -34.73905   4031   0.85   50   70   17.61   1.64   Fnx   17   2M02385365-3433048   39.72355   -34.54810   3918   0.77   39   77   17.85   1.87   Fnx   18   2M02392438-3432530   39.85161   -34.54810   3918   0.79   41   106   17.49   1.99   Fnx   2M02383024-3445030   39.62601   -34.75087   3565   0.24   56   86   17.66   1.95   Fnx   2M02393027807-3431053   39.6702   -34.51817   3922   0.89   55   101   17.63   2.13   Fnx   21   2M02393076-3451354   39.87812   -34.85985   3972   0.96   54   71   17.87   1.86   Fnx   22   2M02394140-3422511   39.92243   -34.348085   3715   0.64   59   72   17.87   1.86   Fnx   22   2M02393198-3419234   39.88329   -34.32318   3495   0.65   54   71   17.83   1.82   Fnx   22   2M02393198-3417028   39.88670   -34.28490   416   1.70   56   101   17.57   2.21   Fnx   22   2M02393285-3417028   39.88670   -34.28490   416   1.70   56   101   17.57   2.21   Fnx   22   2M02394148-342244   40.35363   -34.65363   6557   0.48   40   84   17.77   1.82   Fnx   22   2M02394043-3412351   40.11589   -34.20371   3747   0.63   45   82   17.70   1.89   Fnx   22   2M02395861-3425279   39.99427   -34.42443   3620   0.32   57   140   17.24   2.30   Fnx   23   2M0223934049-3419391   39.91870   -34.20702   4215   1.11   45   75   17.84   1.87   Fnx   32   2M02393365-3424419   39.89019   -34.4165   4519   1.37   42   70   17.86   1.89   Fnx   32   2M02393365-3424419   39.89019   -34.4165   4519   1.37   42   70   17.86   1.89   Fnx   32   2M17185211+5804130   259.71709   58.07026   4888   1.06   -292   107   16.79   1.56   Dra   32   2M17193604-5756289   259.67599   57.98609   4883   1.03   -288   103   16.74   1.53   Dra   2M171915214-5750342   259.80607   58.07026   4888   1.06   -292   107   16.79   1.56   Dra   2M171915214-5750342   259.80604   57.87592   445   0.89   -293   72   17.10   1.47   Dra   2M171915414-5750342   259.80604   57.88510   0.89   -293   72   17.10   1.47   Dra   2M171915415-5756042   260.49254   57.9846   4453   0.84   -302   88   16.67   1.55											
17   2M02385365-3433048   39,72355   -34,55134   3812   0,77   39   77   17,85   1.87   Fnx     18   2M02392438-3432530   39,85161   -34,54810   3918   0,79   41   106   17.49   1.99   Fnx     19   2M02383024-3445030   39,62601   -34,75087   3565   0.24   56   86   17.66   1.95   Fnx     20   2M02372807-3431053   39,36702   -34,51817   3922   0.89   55   101   17.63   2.13   Fnx     21   2M02393076-3431053   39,387812   -34,85985   3972   0.96   54   71   17.87   1.86   Fnx     22   2M023931633432342   39,27432   -34,54286   3733   0.61   46   85   17.69   1.91   Fnx     23   2M02370583-3432342   39,27432   -34,54286   3733   0.61   46   85   17.69   1.91   Fnx     24   2M02393188-3449234   39,88329   -34,32318   3495   0.65   54   71   17.83   1.82   Fnx     25   2M023932823-3417028   39,88670   -34,28409   4126   1.70   56   101   17.57   2.21   Fnx     26   2M023932221-3417028   39,88670   -34,28409   4126   1.70   56   101   17.57   2.21   Fnx     27   2M02384018-3439121   39,66743   -34,65336   6557   0.48   40   84   17.77   1.82   Fnx     28   2M02412486-3422044   40,35363   -34,65336   6557   0.48   40   84   17.77   1.82   Fnx     29   2M02395861-3425279   39,99427   -34,42443   3620   0.32   57   140   17.24   2.30   Fnx     30   2M02402780-3412351   40,11589   -34,20972   4215   1.11   45   75   17.82   1.76   Fnx     31   2M023934049-341991   39,99170   -34,41165   4519   1.37   42   70   17,86   1.89   Fnx     32   2M02393865-3424419   39,89019   -34,41165   4519   1.37   42   70   17,86   1.89   Fnx     33   2M17210223+5815384   260,25928   58,26062   4961   1.06   -274   107   16,71   1.54   Dra     34   2M17193600+5756289   259,90003   57,94136   4810   1.14   -289   73   17,13   1.48   Dra     35   2M17193545+5758465   259,90003   57,94136   4810   1.14   -289   73   17,13   1.48   Dra     36   2M17195544-5759099   259,67599   57,98609   4883   1.03   -288   103   16,74   1.55   Dra     39   2M17191524-5752344   259,90064   57,87592   4437   0.89   -281   78   17,10   1.75   Dra     40   2M17											
18   2M02392483-342530   39.85161   -34.54810   3918   0.79   41   106   17.49   1.99   Fnx     2M02383024-3445030   39.62601   -34.75087   3565   0.24   56   86   17.66   1.95   Fnx     2M02372807-3431053   39.36702   -34.51817   3922   0.89   55   101   17.63   2.13   Fnx     21   2M02393076-3451354   39.87812   -34.85985   3972   0.96   54   71   17.87   1.86   Fnx     22   2M023934140-3422511   39.92243   -34.80858   3715   0.64   59   72   17.87   1.86   Fnx     23   2M02370583-3432342   39.27432   -34.54286   3733   0.61   46   85   17.69   1.91   Fnx     24   2M02393188-3419234   39.88329   -34.32318   3495   0.65   54   71   17.83   1.82   Fnx     25   2M002393285-3417028   39.88670   -34.28409   4126   1.70   56   101   17.57   2.21   Fnx     26   2M0239221-3412133   39.84261   -34.20371   3747   0.63   45   82   17.70   1.89   Fnx     27   2M023934018-349121   39.66743   -34.65336   6357   0.48   40   84   17.77   1.82   Fnx     28   2M02412486-3422044   40.35363   -34.65364   6357   0.48   40   84   17.77   1.82   Fnx     29   2M02395861-3425279   39.99427   -34.42443   3620   0.32   57   140   17.24   2.30   Fnx     30   2M02402780-3412351   40.11589   -34.20972   4215   1.11   45   75   17.84   1.87   Fnx     31   2M02394049-3419391   39.9870   -34.32756   4182   1.13   51   75   17.84   1.87   Fnx     32   2M02393365-3424419   39.89019   -34.41165   4519   1.37   42   70   17.86   1.89   Fnx     33   2M17210223+5815384   260.25928   58.6062   4961   1.06   -274   107   16.71   1.54   Dra     34   2M1719360+5756289   259.90003   57.94136   4810   1.14   -289   73   17.13   1.48   Dra     34   2M1719360+5756289   259.90003   57.94136   4810   1.14   -289   73   17.13   1.48   Dra     35   2M17191225+5802577   259.80107   58.04937   4503   0.99   -281   85   16.97   1.56   Dra     34   2M1719342+5752334   259.86604   57.87592   4437   0.89   -281   78   17.04   1.47   Dra     34   2M1719360+5756042   259.9668   57.87592   4437   0.89   -281   78   17.04   1.47   Dra     34   2M1719360+5756042   260											
19   2M02338302+3445030   39,62601   -34,75087   3565   0,24   56   86   17,66   1,95   Fnx											
20 2M02372807-3431053 39.36702 -34.51817 3922 0.89 55 101 17.63 2.13 Fnx 2M02393076-3451354 39.87812 -34.85985 3972 0.96 54 71 17.87 1.86 Fnx 2M02393196-342511 39.92243 -34.83085 3715 0.64 59 72 17.87 1.86 Fnx 2M02393198-3419234 39.8232 -34.54286 3733 0.61 46 85 17.69 1.91 Fnx 2M02393198-3419234 39.88329 -34.32318 3495 0.65 54 71 17.83 1.82 Fnx 2M02393285-3417028 39.88670 -34.28409 4126 1.70 56 101 17.57 2.21 Fnx 2M02393285-3417028 39.88670 -34.28409 4126 1.70 56 101 17.57 2.21 Fnx 2M02393198-3419234 39.88670 -34.28409 4126 1.70 56 101 17.57 2.21 Fnx 2M02394018-3439121 39.66743 -34.65336 3657 0.48 40 84 17.77 1.89 Fnx 2M02395861-3425279 39.99427 -34.42443 3620 0.32 57 140 17.24 2.30 Fnx 30 2M02402780-3419391 39.91870 -34.32756 4182 1.13 51 75 17.82 1.76 Fnx 31 2M02394049-3419391 39.91870 -34.31756 4182 1.13 51 75 17.82 1.76 Fnx 32 2M02395865-3424419 39.80019 -34.41165 4519 1.37 42 70 17.86 1.89 Fnx 2M17193600+5756289 259.90003 57.94136 4810 1.14 -289 73 17.13 1.48 Dra 32 2M17210223+5815384 260.25928 58.26062 4961 1.06 -274 107 16.71 1.54 Dra 35 2M17193269+5759082 259.90003 57.94609 4883 1.03 -288 103 16.74 1.53 Dra 36 2M1719325+5801357 259.80107 58.04937 4503 0.90 -281 85 16.97 1.45 Dra 38 2M17200396+5750289 259.90003 57.99469 4883 1.03 -288 103 16.74 1.53 Dra 32 M17191225+5802577 259.80107 58.04937 4503 0.90 -281 85 16.97 1.45 Dra 38 2M1720396+5759082 260.01655 57.98564 4209 0.66 -289 110 16.80 1.59 Dra 32 M17191342+575234 259.80604 57.87592 4437 0.89 -281 78 17.04 1.47 Dra 41 2M17195181+5750177 259.96588 57.98564 4209 0.66 -289 110 16.80 1.59 Dra 42 M1719660+5750459 259.96589 57.98569 488 1.03 -280 2.79 85 17.03 1.50 Dra 42 2M17197467+5748365 259.98604 57.87592 4437 0.89 -281 78 17.04 1.47 Dra 42 M171971847+5753045 259.58564 5400 58.585 -300 71 17.16 1.45 Dra 42 M1719767+5748365 259.98604 57.87592 4437 0.89 -282 76 16.99 1.44 Dra 42 M1719767+5748365 259.98609 57.87624 4660 0.99 -282 76 16.99 1.44 Dra 42 M1719767+5748365 259.9866 57.89584 4466 0.98 215 86 1.79 3 1.50 Car 52 M0641218-55033 100.49940 -51.00148 4											
21 2M0239410-3422511 39.92243 -34.85985 3972 0.96 54 71 17.87 1.86 Fnx 22 2M0239410-3422511 39.92243 -34.58085 3715 0.64 59 72 17.87 1.86 Fnx 23 2M02370583-3432342 39.27432 -34.54286 3733 0.61 46 85 17.69 1.91 Fnx 24 2M02393198-3419234 39.88329 -34.32318 3495 0.65 54 71 17.83 1.82 Fnx 25 2M02393285-3417028 39.88670 -34.28409 4126 1.70 56 101 17.57 2.21 Fnx 26 2M0239221-3412133 39.84261 -34.20371 3747 0.63 45 82 17.70 1.89 Fnx 27 2M02384018-3439121 39.66743 -34.65336 3657 0.48 40 84 17.77 1.82 Fnx 28 2M0239281-341233 39.89427 -34.42443 3620 0.32 57 140 17.24 2.30 Fnx 29 2M02395861-3425279 39.99427 -34.42443 3620 0.32 57 140 17.24 2.30 Fnx 30 2M02402780-3412351 40.11589 -34.20972 4215 1.11 45 75 17.82 1.76 Fnx 31 2M02394049-3419391 39.91870 -34.32756 4182 1.13 51 75 17.84 1.87 Fnx 24 2M02393365-3424419 39.89019 -34.41165 4519 1.37 42 70 17.86 1.89 Fnx 24 2M0239365-3424419 39.89019 -34.41165 4519 1.37 42 70 17.86 1.89 Fnx 24 2M17193600+5756289 259.90003 57.98609 4883 1.03 -288 103 16.74 1.53 Dra 2M171912225+5802577 259.80107 58.04937 4503 0.99 -281 85 16.97 1.45 Dra 32 2M17191225+5802577 259.80107 58.04937 4503 0.99 -281 85 16.97 1.45 Dra 32 2M171913245+5752032 260.01655 57.98564 4209 0.66 -289 110 16.80 1.59 Dra 32 2M17191342+5752334 259.80604 57.87592 4437 0.89 -281 178 17.03 1.50 Dra 42 2M17191345+57552345 259.80772 57.97959 4295 0.80 -279 85 17.03 1.50 Dra 42 2M17191345+5752334 259.80604 57.87592 4437 0.89 -281 78 17.03 1.50 Dra 42 2M17191345+5752345 259.80804 57.87592 4437 0.89 -281 78 17.04 1.47 Dra 42 2M1719180807+580168 259.5360 58.02968 4862 1.02 -309 103 16.77 1.50 Dra 42 2M171948675+575935 259.9860 57.87624 4660 0.99 -282 76 16.99 1.44 Dra 42 2M171948675+575935 259.0860 57.87624 4660 0.99 -282 76 16.99 1.44 Dra 42 2M171948767+5748365 259.9868 57.88526 4305 0.85 -300 71 17.10 1.47 Dra 42 2M17194767+5748365 259.9860 57.87624 4660 0.99 -282 76 16.99 1.44 Dra 42 2M17194767+5748365 259.9869 57.89659 4399 0.89 -293 77 17.10 1.47 Dra 42 2M17194767+5748365 259.0866 57.8964 466 0.99 -282 76 16.99 1.44 Dra 42 2M1											
22 2M0(2394140-3422511 39.92243 -34.54286 3733 0.61 46 85 17.69 1.91 Fnx 24 2M0(2393198-3419234 39.88329 -34.52486 3733 0.61 46 85 17.69 1.91 Fnx 39.88329 -34.52480 39.88329 -34.32318 3495 0.65 54 71 17.83 1.82 Fnx 25 2M0(2393285-3417028 39.88670 -34.28409 4126 1.70 56 101 17.57 2.21 Fnx 26 2M0(2392221-3412133 39.84261 -34.20371 3747 0.63 45 82 17.70 1.89 Fnx 27 2M0(2384018-3439121 39.66743 -34.65336 3657 0.48 40 84 17.77 1.82 Fnx 28 2M0(2412486-3422044 40.35363 -34.56794 3705 0.57 63 73 17.79 1.78 Fnx 29 2M0(2395861-3425279 39.99427 -34.42443 3620 0.32 57 140 17.24 2.30 Fnx 30 2M0(2402780-3419391 39.91870 -34.20376 4182 1.11 45 75 17.82 1.76 Fnx 31 2M0(2394049-3419391 39.91870 -34.23756 4182 1.13 51 75 17.84 1.87 Fnx 32 2M0(2393365-3424419 39.89019 -34.41165 4519 1.37 42 70 17.86 1.89 Fnx 32 2M17210223+5815384 260.25928 58.26062 4961 1.06 -274 107 16.71 1.54 Dra 32 2M17184224+5759099 259.90003 57.94136 4810 1.14 -289 73 17.13 1.48 Dra 32 2M17184224+5759099 259.90003 57.94136 4810 1.14 -289 73 17.13 1.48 Dra 32 2M17184224+5759099 259.80107 58.07026 4888 1.03 -288 103 16.74 1.53 Dra 32 2M171935045+5758465 259.89107 58.07026 4888 1.06 -292 107 16.59 1.56 Dra 32 2M17193545+57583465 259.89772 57.98569 4290 0.66 -289 110 16.80 1.59 Dra 32 2M17193545+57583465 259.890772 57.98564 4209 0.66 -289 110 16.80 1.59 Dra 42 2M17193545+57583465 259.89772 57.9959 4295 0.80 -279 85 17.03 1.50 Dra 42 2M17193545+57583465 259.89604 57.87592 4437 0.89 -281 78 17.04 1.47 Dra 42 2M17193645+5758345 259.89605 57.98564 4209 0.66 -289 110 16.80 1.59 Dra 42 2M17193545+5753465 259.89605 57.87624 4660 0.99 -282 76 16.99 1.44 Dra 42 M171251819+5756042 260.49254 57.99459 4399 0.89 -293 72 17.10 1.47 Dra 42 2M17194767+5748365 259.89605 57.87624 4660 0.99 -282 76 16.99 1.44 Dra 42 M171251819+5756042 260.49254 57.99459 4399 0.89 -293 72 17.10 1.47 Dra 42 2M17194767+5748365 259.8960 57.87624 4660 0.99 -282 76 16.99 1.44 Dra 42 M171251819+5756042 260.49254 57.99450 4460 0.99 -282 76 16.99 1.44 Dra 42 M17124767+5748365 259.9860 57.87624 4660 0.99 -2											
23 2M02370583-3432342 39.27432 -34.54286 3733 0.61 46 85 17.69 1.91 Fnx 24 2M02393185-3419234 39.88329 -34.32318 3495 0.65 54 71 17.83 1.82 Fnx 25 2M02393285-3417028 39.88670 -34.28409 4126 1.70 56 101 17.57 2.21 Fnx 26 2M02392221-3412133 39.84261 -34.20371 3747 0.63 45 82 17.70 1.89 Fnx 27 2M02384018-3439121 39.66743 -34.65336 3657 0.48 40 84 17.77 1.82 Fnx 28 2M02412486-3422044 40.53563 -34.36794 3705 0.57 63 73 17.79 1.78 Fnx 29 2M02395861-3425279 39.99427 -34.42443 3620 0.32 57 140 17.24 2.30 Fnx 30 2M02402780-3412351 40.11589 -34.20972 4215 1.11 45 75 17.82 1.76 Fnx 31 2M02394049-3419391 39.91870 -34.32756 4182 1.13 51 75 17.84 1.87 Fnx 32 2M02393365-3424419 39.89019 -34.41165 4519 1.37 42 70 17.86 1.89 Fnx 32 2M171182234-5815384 260.25928 58.26062 4961 1.06 -274 107 16.71 1.54 Dra 2M17193600+5756289 259.90003 57.94136 4810 1.14 -289 73 17.13 1.48 Dra 32 2M17182211+5804130 259.71709 58.07026 4888 1.03 -288 103 16.74 1.53 Dra 32 2M17191225+5802577 259.80107 58.07026 4888 1.06 -292 107 16.79 1.56 Dra 32 2M1719342+5752334 259.80604 57.9959 4295 0.80 -279 85 17.03 1.50 Dra 2M17191342+5752334 259.80604 57.9959 4295 0.80 -279 85 17.03 1.50 Dra 42 2M17193845+5758465 259.89772 57.99509 4883 1.03 -288 103 16.74 1.53 Dra 2M171913425+5759177 259.96588 57.98564 4209 0.66 -289 110 16.80 1.59 Dra 2M17191342+5752334 259.80604 57.87592 4437 0.89 -293 72 17.10 1.47 Dra 42 2M17191341+5759177 259.96588 57.98564 4305 0.85 -300 71 17.16 1.45 Dra 42 2M17195181+5759177 259.96588 57.98564 4305 0.85 -300 71 17.16 1.45 Dra 42 2M17125819+5756042 260.01655 57.98564 4305 0.85 -300 71 17.16 1.45 Dra 44 2M17251819+5756042 260.0469 57.89659 4399 0.89 -293 72 17.10 1.47 Dra 44 2M17251819+5756042 260.0469 57.89659 4399 0.89 -293 72 17.10 1.47 Dra 44 2M17251819+5756042 260.05683 57.89564 4660 0.99 -282 76 16.99 1.44 Dra 42 2M17194767+5756042 260.95683 57.89564 4660 0.99 -282 76 16.99 1.44 Dra 42 2M17194767+5756042 260.95683 57.89564 466 0.98 215 88 17.09 1.65 Car 50.006412612-5055439 100.3581 -50.92886 4466 0.98 215 88 17.15 1.60 Car 50.006											
24         2M02393198-3419234         39.88329         -34.32318         3495         0.65         54         71         17.83         1.82         Fnx           25         2M02393285-3417028         39.88670         -34.28409         4126         1.70         56         101         17.57         2.21         Fnx           26         2M0239221-3412133         39.84261         -34.20371         3747         0.63         45         82         17.70         1.89         Fnx           27         2M0239861-3429214         40.35363         -34.36794         3705         0.57         63         73         17.79         1.78         Fnx           28         2M02412486-3422044         40.35363         -34.36794         3705         0.57         63         73         17.79         1.78         Fnx           30         2M02402780-3412351         40.11589         -34.20972         4215         1.11         45         75         17.82         1.76         Fnx           31         2M0239365-3424419         39.98019         -34.21654         4519         1.37         42         70         7.78         1.89         Fnx           32         2M0239365-3428         299.90003         5											
25 2M02393285-3417028 39.88670 -34.28409 4126 1.70 56 101 17.57 2.21 Fnx 26 2M0239221-3412133 39.84261 -34.20371 3747 0.63 45 82 17.70 1.89 Fnx 27 2M02384018-3439121 39.866743 -34.65336 3657 0.48 40 84 17.77 1.82 Fnx 28 2M02412486-3422044 40.35363 -34.36794 3705 0.57 63 73 17.79 1.78 Fnx 29 2M02395861-3425279 39.99427 -34.42443 3620 0.32 57 140 17.24 2.30 Fnx 30 2M02402780-3412351 40.11589 -34.20972 4215 1.11 45 75 17.82 1.76 Fnx 31 2M02394049-3419391 39.91870 -34.32756 4182 1.13 51 75 17.84 1.87 Fnx 32 2M02393365-3424419 39.89019 -34.41165 4519 1.37 42 70 17.86 1.89 Fnx 33 2M17210223+5815384 260.25928 58.26062 4961 1.06 -274 107 16.71 1.54 Dra 34 2M17193600+5756289 259.90003 57.94136 4810 1.14 -289 73 17.13 1.48 Dra 35 2M17184224+5759099 259.67599 57.98609 4883 1.03 -288 103 16.74 1.53 Dra 36 2M17185211+5804130 259.71709 58.07026 4888 1.06 -292 107 16.79 1.56 Dra 37 2M17191225+5802577 259.80107 58.04937 4503 0.90 -281 85 16.97 1.45 Dra 38 2M17200396+5759082 260.01655 57.98564 4209 0.66 -289 110 16.80 1.59 Dra 39 2M1719134575752334 259.80604 57.87592 4437 0.89 -281 78 17.04 1.47 Dra 40 2M171913427552334 259.80604 57.87592 4437 0.89 -281 78 17.04 1.47 Dra 41 2M17195181+5759177 259.96588 57.98564 4209 0.66 -289 110 16.80 1.59 Dra 42 2M17180807+5801468 259.53360 58.02968 4862 1.02 -309 103 16.77 1.50 Dra 44 2M17205204+5759477 260.21692 57.99659 4399 0.89 -293 72 17.10 1.47 Dra 44 2M17205204+5759477 260.21692 57.99659 4399 0.89 -293 72 17.10 1.47 Dra 44 2M17215819+5755042 260.49254 57.93446 4453 0.84 -302 78 16.99 1.44 Dra 45 2M17205204+5759477 260.21692 57.99659 4399 0.89 -293 72 17.10 1.47 Dra 46 2M17162365+5752345 259.90860 57.87624 4660 0.99 -282 76 16.99 1.44 Dra 47 2M17194767+5748365 259.94869 57.81015 4465 0.81 -282 88 16.66 1.53 Dra 48 2M06415460-5057007 100.47748 -50.95019 4309 0.87 232 78 17.09 1.65 Car 49 2M06412828-510038 100.61778 -51.00108 4660 1.14 214 82 17.28 1.58 Car 51 2M06422826-5100038 100.61778 -51.00108 4660 1.14 214 82 17.28 1.55 Car 52 2M06420106-5103442 100.50446 -51.00628 4319 0.96 225 71											
26         2M02392221-3412133         39.84261         -34.20371         3747         0.63         45         82         17.70         1.89         Fnx           27         2M02384018-3439121         39.66743         -34.65336         3657         0.48         40         84         17.77         1.82         Fnx           28         2M02412486-3422044         40.35363         -34.36794         3705         0.57         63         73         17.79         1.78         Fnx           29         2M02395861-3425279         39.99427         -34.42443         3620         0.32         57         140         17.24         2.30         Fnx           30         2M02402780-3412351         40.11589         -34.20972         4215         1.11         45         75         17.84         1.87         Fnx           31         2M02393465-3424419         39.98019         -34.4165         4519         1.37         42         70         17.86         1.89         Fnx           32         2M07210223+5815384         260.25928         58.26062         4961         1.06         -274         107         16.71         1.54         Dra           34         2M1718521+5802457         259.67599											
27         2M02384018-3439121         39.66743         -34.65336         3657         0.48         40         84         17.77         1.82         Fnx           28         2M02412486-3422044         40.35363         -34.36794         3705         0.57         63         73         17.79         1.78         Fnx           30         2M02395861-3425279         39.99427         -34.24443         3620         0.32         57         140         17.24         2.30         Fnx           30         2M023934049-3419391         39.991870         -34.32756         4182         1.13         51         75         17.84         1.87         Fnx           31         2M02393365-3424419         39.89019         -34.41165         4519         1.37         42         70         17.86         1.89         Fnx           32         2M0239365-3424419         39.89019         -34.41165         4519         1.37         42         70         17.86         1.89         Fnx           32         2M17193600+5756289         259.90003         57.94136         4810         1.14         -289         73         17.13         1.48         Dra           35         2M17186211+5804130         259.71709											
28 2M02412486-3422044											
29 2M02395861-3425279 39.99427 -34.42443 3620 0.32 57 140 17.24 2.30 Fnx 30 2M02402780-3412351 40.11589 -34.20972 4215 1.11 45 75 17.82 1.76 Fnx 31 2M02394049-3419391 39.91870 -34.32756 4182 1.13 51 75 17.84 1.87 Fnx 32 2M02393365-3424419 39.89019 -34.41165 4519 1.37 42 70 17.86 1.89 Fnx 33 2M17210223+5815384 260.25928 58.26062 4961 1.06 -274 107 16.71 1.54 Dra 34 2M17193600+5756289 259.90003 57.94136 4810 1.14 -289 73 17.13 1.48 Dra 35 2M17184224+5759099 259.67599 57.98609 4883 1.03 -288 103 16.74 1.53 Dra 36 2M17185211+5804130 259.71709 58.07026 4888 1.03 -288 103 16.74 1.53 Dra 37 2M17191225+5802577 259.80107 58.04937 4503 0.90 -281 85 16.97 1.45 Dra 38 2M17200396+5759082 260.01655 57.98564 4209 0.66 -289 110 16.80 1.59 Dra 39 2M17193545+5758465 259.89772 57.97959 4295 0.80 -279 85 17.03 1.50 Dra 40 2M17191342+5752344 259.80604 57.87592 4437 0.89 -281 78 17.04 1.47 Dra 41 2M17195181+5759177 259.96588 57.98826 4305 0.85 -300 71 17.16 1.45 Dra 42 2M17180807+5801468 259.53360 58.02968 4862 1.02 -309 103 16.77 1.50 Dra 43 2M17205204+5759477 260.21692 57.99659 4399 0.89 -293 72 17.10 1.47 Dra 44 2M17215819+5756042 260.49254 57.93446 4453 0.84 -302 78 16.91 1.44 Dra 45 2M17162365+5752345 259.09860 57.87624 4660 0.99 -282 76 16.99 1.44 Dra 46 2M17162365+5752345 259.09860 57.87624 4660 0.99 -282 76 16.99 1.44 Dra 47 2M17194767+5748365 259.94869 57.8810 4150 0.64 -302 80 16.89 1.49 Dra 48 2M06415460-5057007 100.47748 -50.95019 4309 0.87 232 78 17.10 1.47 Dra 49 2M0641282-65100038 100.61778 -51.00108 4660 1.14 214 82 17.28 1.58 Car 50 2M06420106-5103442 100.50446 -51.06228 4319 0.96 225 71 17.38 1.50 Car 51 2M06422826-5100038 100.61778 -51.00108 4660 1.14 214 82 17.28 1.58 Car 52 2M06420106-5103442 100.50446 -51.06228 4319 0.96 225 71 17.38 1.50 Car 53 2M06412718-510182 100.36326 -51.00510 4507 1.05 233 78 17.29 1.53 Car											
30 2M02402780-3412351											
31 2M02394049-3419391 39.91870 -34.32756 4182 1.13 51 75 17.84 1.87 Fnx 32 2M02393365-3424419 39.89019 -34.41165 4519 1.37 42 70 17.86 1.89 Fnx 33 2M17210223+5815384 260.25928 58.26062 4961 1.06 -274 107 16.71 1.54 Dra 34 2M17193600+5756289 259.90003 57.94136 4810 1.14 -289 73 17.13 1.48 Dra 35 2M17184224+5759099 259.67599 57.98609 4883 1.03 -288 103 16.74 1.53 Dra 36 2M17185211+5804130 259.71709 58.07026 4888 1.06 -292 107 16.79 1.56 Dra 37 2M17191225+5802577 259.80107 58.04937 4503 0.90 -281 85 16.97 1.45 Dra 38 2M17200396+5759082 260.01655 57.98564 4209 0.66 -289 1110 16.80 1.59 Dra 39 2M17193454+57584465 259.89772 57.97959 4295 0.80 -279 85 17.03 1.50 Dra 40 2M17191342+5752334 259.80604 57.87592 4437 0.89 -281 78 17.04 1.47 Dra 41 2M17195181+5759177 259.96588 57.9826 4305 0.85 -300 71 17.16 1.45 Dra 42 2M17180807+5801468 259.53360 58.02968 4862 1.02 -309 103 16.77 1.50 Dra 43 2M17205204+5759477 260.21692 57.99659 4399 0.89 -293 72 17.10 1.47 Dra 44 2M17215819+5756042 260.49254 57.93446 4453 0.84 -302 78 16.91 1.44 Dra 45 2M17221363+5753065 260.55683 57.88510 4150 0.64 -302 80 16.89 1.49 Dra 46 2M17162365+5752345 259.98606 57.87624 4660 0.99 -282 76 16.99 1.44 Dra 47 2M17194767+5748365 259.98869 57.881015 4465 0.81 -280 88 16.76 1.53 Dra 48 2M06415460-5057007 100.47748 -50.95019 4309 0.87 232 78 17.09 1.65 Car 50 2M0641282-5510038 100.45096 -50.91713 4587 1.05 224 88 17.15 1.60 Car 51 2M06422826-5100038 100.45096 -50.91713 4587 1.05 224 88 17.15 1.60 Car 52 2M06420106-5103442 100.50446 -51.06228 4319 0.96 225 71 17.38 1.50 Car 53 2M06420106-5103442 100.50446 -51.06228 4319 0.96 225 71 17.38 1.50 Car 54 2M06415858-5101533 100.49940 -51.03147 4801 1.16 217 93 17.11 1.62 Car 54 2M06412718-5100182 100.36326 -51.00510 4507 1.05 233 78 17.29 1.53 Car											
32         2M02393365-3424419         39.89019         -34.41165         4519         1.37         42         70         17.86         1.89         Fnx           33         2M17210223+5815384         260.25928         58.26062         4961         1.06         -274         107         16.71         1.54         Dra           34         2M17193600+5756289         259.90003         57.94136         4810         1.14         -289         73         17.13         1.48         Dra           35         2M17194224+5759099         259.67599         57.98609         4883         1.03         -288         103         16.74         1.53         Dra           36         2M17185211+5804130         259.71709         58.07026         4888         1.06         -292         107         16.79         1.56         Dra           37         2M17191225+5802577         259.80107         58.04937         4503         0.90         -281         85         16.97         1.45         Dra           38         2M1720396+5759082         260.01655         57.98564         4209         0.66         -289         110         16.80         1.59         Dra           40         2M1719342+5755245         259.897											
33 2M17210223+5815384 260.25928 58.26062 4961 1.06 -274 107 16.71 1.54 Dra 34 2M17193600+5756289 259.90003 57.94136 4810 1.14 -289 73 17.13 1.48 Dra 35 2M17184224+5759099 259.67599 57.98609 4883 1.03 -288 103 16.74 1.53 Dra 36 2M17185211+5804130 259.71709 58.07026 4888 1.06 -292 107 16.79 1.56 Dra 37 2M17191225+5802577 259.80107 58.04937 4503 0.90 -281 85 16.97 1.45 Dra 38 2M17200396+5759082 260.01655 57.98564 4209 0.66 -289 110 16.80 1.59 Dra 39 2M17193545+5758465 259.89772 57.97959 4295 0.80 -279 85 17.03 1.50 Dra 40 2M17191342+5752334 259.80604 57.87592 4437 0.89 -281 78 17.04 1.47 Dra 41 2M17195181+5759177 259.96588 57.9826 4305 0.85 -300 71 17.16 1.45 Dra 42 2M17180807+5801468 259.53360 58.02968 4862 1.02 -309 103 16.77 1.50 Dra 43 2M17205204+5759477 260.21692 57.99659 4399 0.89 -293 72 17.10 1.47 Dra 44 2M17215819+5756042 260.49254 57.93446 4453 0.84 -302 78 16.91 1.44 Dra 45 2M17221363+5752345 259.09860 57.88510 4150 0.64 -302 80 16.89 1.49 Dra 46 2M17162365+5752345 259.09860 57.87624 4660 0.99 -282 76 16.99 1.44 Dra 47 2M17194767+5748365 259.94869 57.81015 4465 0.81 -280 88 16.76 1.53 Dra 48 2M06415460-5057007 100.47748 -50.95019 4309 0.87 232 78 17.10 1.67 Dra 49 2M06414823-5055016 100.45096 -50.91713 4587 1.05 224 88 17.15 1.60 Car 50 2M06412612-5055439 100.35881 -50.92886 4466 0.98 215 86 17.16 1.57 Car 51 2M06422826-5100038 100.61778 -51.00108 4660 1.14 214 82 17.28 1.58 Car 52 2M0642106-5103442 100.50446 -51.06228 4319 0.96 225 71 17.38 1.50 Car 53 2M06415985-5101533 100.49940 -51.03147 4801 1.16 217 93 17.11 1.62 Car 54 2M06412718-5100182 100.36326 -51.00510 4507 1.05 233 78 17.29 1.53 Car											
34         2M17193600+5756289         259.90003         57.94136         4810         1.14         -289         73         17.13         1.48         Dra           35         2M17184224+5759099         259.67599         57.98609         4883         1.03         -288         103         16.74         1.53         Dra           36         2M17185211+5804130         259.71709         58.07026         4888         1.06         -292         107         16.79         1.56         Dra           37         2M17191225+5802577         259.80107         58.04937         4503         0.90         -281         85         16.97         1.45         Dra           38         2M17200396+5759082         260.01655         57.98564         4209         0.66         -289         110         16.80         1.59         Dra           39         2M1719342+5752846         259.89772         57.97594         4295         0.80         -279         85         17.03         1.50         Dra           40         2M1719342+5752344         259.80604         57.87592         4437         0.89         -281         78         17.04         1.47         Dra           41         2M1719581+5750472         259.953											
35         2M17184224+5759099         259.67599         57.98609         4883         1.03         -288         103         16.74         1.53         Dra           36         2M17185211+5804130         259.71709         58.07026         4888         1.06         -292         107         16.79         1.56         Dra           37         2M17191225+5802577         259.80107         58.04937         4503         0.90         -281         85         16.97         1.45         Dra           38         2M17200396+5759082         260.01655         57.98564         4209         0.66         -289         110         16.80         1.59         Dra           39         2M17193545+5758465         259.89772         57.97959         4295         0.80         -279         85         17.03         1.50         Dra           40         2M1719342+5752334         259.80604         57.87592         4437         0.89         -281         78         17.04         1.47         Dra           41         2M1719581+5759177         259.96588         57.98826         4305         0.85         -300         71         17.16         1.45         Dra           42         2M17180807+5801468         259.53											
36         2M17185211+5804130         259.71709         58.07026         4888         1.06         -292         107         16.79         1.56         Dra           37         2M17191225+5802577         259.80107         58.04937         4503         0.90         -281         85         16.97         1.45         Dra           38         2M17200396+5759082         260.01655         57.98564         4209         0.66         -289         110         16.80         1.59         Dra           39         2M17193545+5758465         259.89772         57.97959         4295         0.80         -279         85         17.03         1.50         Dra           40         2M17191342+5752334         259.80604         57.87592         4437         0.89         -281         78         17.04         1.47         Dra           41         2M17195181+5759177         259.96588         57.98264         4305         0.85         -300         71         17.16         1.45         Dra           42         2M17180807+5801468         259.53360         58.02968         4862         1.02         -309         103         16.77         1.50         Dra           43         2M17205204+5759477         260.											
37         2M17191225+5802577         259.80107         58.04937         4503         0.90         -281         85         16.97         1.45         Dra           38         2M17200396+5759082         260.01655         57.98564         4209         0.66         -289         110         16.80         1.59         Dra           39         2M17193545+5758465         259.89772         57.97959         4295         0.80         -279         85         17.03         1.50         Dra           40         2M17191342+5752334         259.80604         57.87592         4437         0.89         -281         78         17.04         1.47         Dra           41         2M17195181+5759177         259.96588         57.98826         4305         0.85         -300         71         17.16         1.45         Dra           42         2M17180807+5801468         259.53360         58.02968         4862         1.02         -309         103         16.77         1.50         Dra           43         2M17205204+5759477         260.21692         57.99659         4399         0.89         -293         72         17.10         1.47         Dra           45         2M172218619+5756042         260.											
38 2M17200396+5759082 260.01655 57.98564 4209 0.66 -289 110 16.80 1.59 Dra 39 2M17193545+5758465 259.89772 57.97959 4295 0.80 -279 85 17.03 1.50 Dra 40 2M17191342+5752334 259.80604 57.87592 4437 0.89 -281 78 17.04 1.47 Dra 41 2M17195181+5759177 259.96588 57.98826 4305 0.85 -300 71 17.16 1.45 Dra 42 2M17180807+5801468 259.53360 58.02968 4862 1.02 -309 103 16.77 1.50 Dra 43 2M17205204+5759477 260.21692 57.99659 4399 0.89 -293 72 17.10 1.47 Dra 44 2M17215819+5756042 260.49254 57.93446 4453 0.84 -302 78 16.91 1.44 Dra 45 2M17221363+5753065 260.55683 57.88510 4150 0.64 -302 80 16.89 1.49 Dra 46 2M17162365+5752345 259.09860 57.87624 4660 0.99 -282 76 16.99 1.44 Dra 47 2M17194767+5748365 259.94869 57.81015 4465 0.81 -280 88 16.76 1.53 Dra 48 2M06415460-5057007 100.47748 -50.95019 4309 0.87 232 78 17.09 1.65 Car 49 2M06412612-5055439 100.35881 -50.92886 4466 0.98 215 86 17.16 1.57 Car 50 2M06412612-5055439 100.35881 -50.92886 4466 0.98 215 86 17.16 1.57 Car 51 2M06422826-5100038 100.61778 -51.00108 4660 1.14 214 82 17.28 1.58 Car 52 2M06420106-5103442 100.50446 -51.06228 4319 0.96 225 71 17.38 1.50 Car 53 2M06415985-5101533 100.49940 -51.03147 4801 1.16 217 93 17.11 1.62 Car 54 2M06412718-5100182 100.36326 -51.00510 4507 1.05 233 78 17.29 1.53 Car											
39 2M17193545+5758465 259.89772 57.97959 4295 0.80 -279 85 17.03 1.50 Dra 40 2M17191342+5752334 259.80604 57.87592 4437 0.89 -281 78 17.04 1.47 Dra 41 2M17195181+5759177 259.96588 57.98826 4305 0.85 -300 71 17.16 1.45 Dra 42 2M17180807+5801468 259.53360 58.02968 4862 1.02 -309 103 16.77 1.50 Dra 43 2M17205204+5759477 260.21692 57.99659 4399 0.89 -293 72 17.10 1.47 Dra 44 2M17215819+5756042 260.49254 57.93446 4453 0.84 -302 78 16.91 1.44 Dra 45 2M17221363+5753065 260.55683 57.88510 4150 0.64 -302 80 16.89 1.49 Dra 46 2M17162365+5752345 259.09860 57.87624 4660 0.99 -282 76 16.99 1.44 Dra 47 2M17194767+5748365 259.94869 57.81015 4465 0.81 -280 88 16.76 1.53 Dra 48 2M06415460-5057007 100.47748 -50.95019 4309 0.87 232 78 17.09 1.65 Car 49 2M06414823-5055016 100.45096 -50.91713 4587 1.05 224 88 17.15 1.60 Car 50 2M06412612-5055439 100.35881 -50.92886 4466 0.98 215 86 17.16 1.57 Car 51 2M06422826-5100038 100.61778 -51.00108 4660 1.14 214 82 17.28 1.58 Car 52 2M06420106-5103442 100.50446 -51.06228 4319 0.96 225 71 17.38 1.50 Car 53 2M06415985-5101533 100.49940 -51.03147 4801 1.16 217 93 17.11 1.62 Car 54 2M06412718-5100182 100.36326 -51.00510 4507 1.05 233 78 17.29 1.53 Car											
40       2M17191342+5752334       259.80604       57.87592       4437       0.89       -281       78       17.04       1.47       Dra         41       2M17195181+5759177       259.96588       57.98826       4305       0.85       -300       71       17.16       1.45       Dra         42       2M17180807+5801468       259.53360       58.02968       4862       1.02       -309       103       16.77       1.50       Dra         43       2M17205204+5759477       260.21692       57.99659       4399       0.89       -293       72       17.10       1.47       Dra         44       2M17215819+5756042       260.49254       57.93446       4453       0.84       -302       78       16.91       1.44       Dra         45       2M17221363+5753065       260.55683       57.88510       4150       0.64       -302       80       16.89       1.49       Dra         46       2M17162365+5752345       259.99860       57.87624       4660       0.99       -282       76       16.99       1.44       Dra         47       2M17194767+5748365       259.94869       57.81015       4465       0.81       -280       88       16.76       1.53 <td></td>											
41       2M17195181+5759177       259.96588       57.98826       4305       0.85       -300       71       17.16       1.45       Dra         42       2M17180807+5801468       259.53360       58.02968       4862       1.02       -309       103       16.77       1.50       Dra         43       2M17205204+5759477       260.21692       57.99659       4399       0.89       -293       72       17.10       1.47       Dra         44       2M17215819+5756042       260.49254       57.93446       4453       0.84       -302       78       16.91       1.44       Dra         45       2M17221363+5753065       260.55683       57.88510       4150       0.64       -302       80       16.89       1.49       Dra         46       2M17162365+5752345       259.09860       57.87624       4660       0.99       -282       76       16.99       1.44       Dra         47       2M17194767+5748365       259.94869       57.81015       4465       0.81       -280       88       16.76       1.53       Dra         48       2M06415460-5057007       100.47748       -50.95019       4309       0.87       232       78       17.09       1.65 <td></td>											
42       2M17180807+5801468       259.53360       58.02968       4862       1.02       -309       103       16.77       1.50       Dra         43       2M17205204+5759477       260.21692       57.99659       4399       0.89       -293       72       17.10       1.47       Dra         44       2M17215819+5756042       260.49254       57.93446       4453       0.84       -302       78       16.91       1.44       Dra         45       2M17221363+5753065       260.55683       57.88510       4150       0.64       -302       80       16.89       1.49       Dra         46       2M17162365+5752345       259.09860       57.87624       4660       0.99       -282       76       16.99       1.44       Dra         47       2M17194767+5748365       259.94869       57.81015       4465       0.81       -280       88       16.76       1.53       Dra         48       2M06415460-5057007       100.47748       -50.95019       4309       0.87       232       78       17.09       1.65       Car         50       2M06412612-5055439       100.35881       -50.92886       4466       0.98       215       86       17.16       1.57 <td></td> <td></td> <td></td> <td></td> <td></td> <td></td> <td></td> <td></td> <td>17.16</td> <td></td> <td></td>									17.16		
43       2M17205204+5759477       260.21692       57.99659       4399       0.89       -293       72       17.10       1.47       Dra         44       2M17215819+5756042       260.49254       57.93446       4453       0.84       -302       78       16.91       1.44       Dra         45       2M17221363+5753065       260.55683       57.88510       4150       0.64       -302       80       16.89       1.49       Dra         46       2M17162365+5752345       259.09860       57.87624       4660       0.99       -282       76       16.99       1.44       Dra         47       2M17194767+5748365       259.94869       57.81015       4465       0.81       -280       88       16.76       1.53       Dra         48       2M06415460-5057007       100.47748       -50.95019       4309       0.87       232       78       17.09       1.65       Car         49       2M06414823-5055016       100.45096       -50.91713       4587       1.05       224       88       17.15       1.60       Car         50       2M06422826-5100038       100.61778       -51.00108       4660       1.14       214       82       17.28       1.58											
44       2M17215819+5756042       260.49254       57.93446       4453       0.84       -302       78       16.91       1.44       Dra         45       2M17221363+5753065       260.55683       57.88510       4150       0.64       -302       80       16.89       1.49       Dra         46       2M17162365+5752345       259.09860       57.87624       4660       0.99       -282       76       16.99       1.44       Dra         47       2M17194767+5748365       259.94869       57.81015       4465       0.81       -280       88       16.76       1.53       Dra         48       2M06415460-5057007       100.47748       -50.95019       4309       0.87       232       78       17.09       1.65       Car         49       2M06414823-5055016       100.45096       -50.91713       4587       1.05       224       88       17.15       1.60       Car         50       2M06412612-5055439       100.35881       -50.92886       4466       0.98       215       86       17.16       1.57       Car         51       2M06422826-5100038       100.61778       -51.00108       4660       1.14       214       82       17.28       1.58											
45 2M17221363+5753065 260.55683 57.88510 4150 0.64 -302 80 16.89 1.49 Dra 46 2M17162365+5752345 259.09860 57.87624 4660 0.99 -282 76 16.99 1.44 Dra 47 2M17194767+5748365 259.94869 57.81015 4465 0.81 -280 88 16.76 1.53 Dra 48 2M06415460-5057007 100.47748 -50.95019 4309 0.87 232 78 17.09 1.65 Car 49 2M06414823-5055016 100.45096 -50.91713 4587 1.05 224 88 17.15 1.60 Car 50 2M06412612-5055439 100.35881 -50.92886 4466 0.98 215 86 17.16 1.57 Car 51 2M06422826-5100038 100.61778 -51.00108 4660 1.14 214 82 17.28 1.58 Car 52 2M06420106-5103442 100.50446 -51.06228 4319 0.96 225 71 17.38 1.50 Car 53 2M06415985-5101533 100.49940 -51.03147 4801 1.16 217 93 17.11 1.62 Car 54 2M06412718-5100182 100.36326 -51.00510 4507 1.05 233 78 17.29 1.53 Car											
46       2M17162365+5752345       259.09860       57.87624       4660       0.99       -282       76       16.99       1.44       Dra         47       2M17194767+5748365       259.94869       57.81015       4465       0.81       -280       88       16.76       1.53       Dra         48       2M06415460-5057007       100.47748       -50.95019       4309       0.87       232       78       17.09       1.65       Car         49       2M06414823-5055016       100.45096       -50.91713       4587       1.05       224       88       17.15       1.60       Car         50       2M06412612-5055439       100.35881       -50.92886       4466       0.98       215       86       17.16       1.57       Car         51       2M06422826-5100038       100.61778       -51.00108       4660       1.14       214       82       17.28       1.58       Car         52       2M06420106-5103442       100.50446       -51.06228       4319       0.96       225       71       17.38       1.50       Car         53       2M06415985-5101533       100.49940       -51.03147       4801       1.16       217       93       17.11       1.62											
47       2M17194767+5748365       259.94869       57.81015       4465       0.81       -280       88       16.76       1.53       Dra         48       2M06415460-5057007       100.47748       -50.95019       4309       0.87       232       78       17.09       1.65       Car         49       2M06414823-5055016       100.45096       -50.91713       4587       1.05       224       88       17.15       1.60       Car         50       2M06412612-5055439       100.35881       -50.92886       4466       0.98       215       86       17.16       1.57       Car         51       2M06422826-5100038       100.61778       -51.00108       4660       1.14       214       82       17.28       1.58       Car         52       2M06420106-5103442       100.50446       -51.06228       4319       0.96       225       71       17.38       1.50       Car         53       2M06415985-5101533       100.49940       -51.03147       4801       1.16       217       93       17.11       1.62       Car         54       2M06412718-5100182       100.36326       -51.00510       4507       1.05       233       78       17.29       1.53											
48 2M06415460-5057007 100.47748 -50.95019 4309 0.87 232 78 17.09 1.65 Car 49 2M06414823-5055016 100.45096 -50.91713 4587 1.05 224 88 17.15 1.60 Car 50 2M06412612-5055439 100.35881 -50.92886 4466 0.98 215 86 17.16 1.57 Car 51 2M06422826-5100038 100.61778 -51.00108 4660 1.14 214 82 17.28 1.58 Car 52 2M06420106-5103442 100.50446 -51.06228 4319 0.96 225 71 17.38 1.50 Car 53 2M06415985-5101533 100.49940 -51.03147 4801 1.16 217 93 17.11 1.62 Car 54 2M06412718-5100182 100.36326 -51.00510 4507 1.05 233 78 17.29 1.53 Car											
50       2M06412612-5055439       100.35881       -50.92886       4466       0.98       215       86       17.16       1.57       Car         51       2M06422826-5100038       100.61778       -51.00108       4660       1.14       214       82       17.28       1.58       Car         52       2M06420106-5103442       100.50446       -51.06228       4319       0.96       225       71       17.38       1.50       Car         53       2M06415985-5101533       100.49940       -51.03147       4801       1.16       217       93       17.11       1.62       Car         54       2M06412718-5100182       100.36326       -51.00510       4507       1.05       233       78       17.29       1.53       Car		2M06415460-5057007		-50.95019							
50       2M06412612-5055439       100.35881       -50.92886       4466       0.98       215       86       17.16       1.57       Car         51       2M06422826-5100038       100.61778       -51.00108       4660       1.14       214       82       17.28       1.58       Car         52       2M06420106-5103442       100.50446       -51.06228       4319       0.96       225       71       17.38       1.50       Car         53       2M06415985-5101533       100.49940       -51.03147       4801       1.16       217       93       17.11       1.62       Car         54       2M06412718-5100182       100.36326       -51.00510       4507       1.05       233       78       17.29       1.53       Car	49	2M06414823-5055016	100.45096	-50.91713	4587	1.05	224	88	17.15	1.60	Car
51       2M06422826-5100038       100.61778       -51.00108       4660       1.14       214       82       17.28       1.58       Car         52       2M06420106-5103442       100.50446       -51.06228       4319       0.96       225       71       17.38       1.50       Car         53       2M06415985-5101533       100.49940       -51.03147       4801       1.16       217       93       17.11       1.62       Car         54       2M06412718-5100182       100.36326       -51.00510       4507       1.05       233       78       17.29       1.53       Car	50	2M06412612-5055439	100.35881	-50.92886	4466	0.98	215	86	17.16	1.57	
53 2M06415985-5101533 100.49940 -51.03147 4801 1.16 217 93 17.11 1.62 Car 54 2M06412718-5100182 100.36326 -51.00510 4507 1.05 233 78 17.29 1.53 Car			100.61778	-51.00108	4660	1.14	214	82	17.28	1.58	Car
54 2M06412718-5100182 100.36326 -51.00510 4507 1.05 233 78 17.29 1.53 Car					4319						
				-51.03147	4801				17.11		
55 2M06411470-5051099 100.31128 -50.85277 4056 0.70 220 73 17.23 1.49 Car											
	_55	2M06411470-5051099	100.31128	-50.85277	4056	0.70	220	73	17.23	1.49	Car

#	APOGEE ID	RA [deg]	DEC [deg]	$T_{\text{eff}} = \log g$ [K]		<i>RV</i> [km s <sup>-1</sup> ]	S/N	Gmag [mag]	BP-RP [mag]	Dwarf Galaxy
56	2M06415969-5051133	100.49872	-50.85368	3714	0.35	211	73	17.30	1.56	Car
57	2M06413963-5049587	100.41515	-50.83298	4652	1.09	230	84	17.14	1.58	Car
58	2M06403111-5055246	100.12971	-50.92348	5029	1.34	213	74	17.33	1.51	Car
59	2M06410537-5105257	100.27240	-51.09047	4243	0.81	227	96	17.10	1.57	Car
60	2M06411566-5059480	100.31527	-50.99668	4074	0.77	227	78	17.37	1.53	Car
61	2M06405789-5102276	100.24127	-51.04100	4447	1.00	226	70	17.30	1.44	Car
62	2M06403082-5059153	100.12848	-50.98756	3777	0.44	217	74	17.32	1.52	Car
63	2M06404635-5101392	100.19319	-51.02753	4975	1.27	230	79	17.22	1.53	Car
64	2M06410501-5101359	100.27090	-51.02663	4532	1.02	221	94	17.15	1.58	Car
65	2M06404775-5106033	100.19901	-51.10094	4335	0.88	236	89	17.11	1.59	Car
66	2M06411676-5100540	100.31984	-51.01501	4048	0.74	221	70	17.35	1.48	Car
67	2M10143985-0110527	153.66609	-1.18129	4506	1.19	239	54	17.32	1.50	Sex
68	2M10133675-0108018	153.40315	-1.13382	4699	0.72	235	74	16.75	1.53	Sex
69	2M10143342-0135549	153.63932	-1.59858	4631	1.19	216	42	17.42	1.46	Sex
70	2M10111188-0148488	152.79948	-1.81351	5001	1.48	228	65	17.14	1.48	Sex
71	2M10135723-0144452	153.48848	-1.74586	4711	1.03	218	57	17.48	1.44	Sex
72	2M10121613-0145482	153.06727	-1.76341	3990	1.16	221	71	17.25	1.49	Sex
73	2M10133529-0117548	153.39708	-1.29854	4308	1.03	227	50	17.32	1.47	Sex
74	2M10122523-0122257	153.10512	-1.37386	4316	0.63	220	88	16.79	1.64	Sex

**Table A.2.** Chemical abundance of all sample stars

#	[Fe/H]	[C/Fe]	[N/Fe]	[O/Fe]	[Mg/Fe]	[Al/Fe]	[Si/Fe]	[Ca/Fe]	[Ti/Fe]	[Cr/Fe]	[Mn/Fe]	[Ni/Fe]	[Ce/Fe]
1	-1.65			-0.13	0.11	-0.47	0.28	0.15					
2	-1.32					-0.89	-0.08						-0.07
3	-1.21	0.45	0.56	0.35	0.29	-0.42	0.39	0.14	0.04			0.11	0.19
4	-1.12			0.05	-0.09	-0.81	0.07	-0.09	-0.51		-0.16		0.14
5	-1.1			-0.31	-0.05	-0.43	0.18	0.04	0.22	-0.27	-0.04		0.26
6	-1.07	0.05	-0.13	0.27	-0.07	-0.5	0.11	0.09	-0.24	-0.33	-0.15	-0.01	0.18
7	-1.04	-0.47	0.36	-0.06		-0.46	0.03	-0.01	0.15	0.03	-0.25		0.32
8	-1.01	-0.13	0.07	0.21		-0.8	0.12	-0.03	-0.29	-0.15	-0.17	0.09	0.32
9	-0.99			0.47	-0.13	-0.32	0.15	0.24	0.14	0.14	-0.09	-0.37	0.46
10	-0.98	-0.52	1.23	0.46	-0.19	-0.38	-0.05		0.0	-0.14	-0.32	•••	0.07
11	-0.97					•••	0.06		0.3		-0.19	•••	-0.17
12	-0.96	-0.08	0.22	0.25	-0.27	-0.74	-0.04	-0.06	-0.27	•••	-0.25	•••	0.3
13	-0.94			0.43	-0.43	-0.3	-0.08	0.14	0.22	0.04	-0.23		0.37
14	-0.93	-0.41	0.45	0.03	-0.13	-0.29	0.13	-0.04	-0.07	-0.5	-0.25		0.36
15	-0.92	-0.36	0.36	0.26	-0.33	-0.61	-0.06	-0.13	-0.02	-0.21	-0.27	-0.16	0.14
16	-0.91			0.31	0.01	-0.3	0.12	0.13	0.26	-0.02	-0.18		
17	-0.9	-0.51	-0.01	0.05	-0.18	-0.51	0.01	-0.15	-0.33	-0.02	-0.22		0.16
18	-0.89	-0.1	0.67	0.51	-0.18	-0.35	0.0	-0.06	-0.17	-0.3	-0.32	-0.21	0.3
19	-0.85	-0.77	0.27	-0.06	-0.15	•••	-0.03	-0.36	-0.37	-0.56	-0.41	-0.39	-0.13
20	-0.81	-0.42	0.94	0.54	-0.35	-0.44	-0.05	0.01	0.22		-0.23	-0.36	0.32
21	-0.8	-0.4	0.68	0.36	-0.17	-0.64	0.03	-0.11	-0.12	-0.36	-0.18	-0.48	0.31
22	-0.79	•••	•••	-0.19	-0.41	-0.58	-0.02	-0.1	-0.17	•••	-0.36	•••	0.03
23	-0.77		•••	-0.08	-0.27	-0.56	0.11	-0.14	-0.27	-0.37	-0.41	-0.26	0.11
24	-0.76	-1.22	0.4	-0.54	0.0	-0.68	0.27	-0.22	-0.04	•••	-0.48	-0.31	-0.12
25	-0.73	-0.02	0.74	0.91	-0.34	-0.35	0.05	0.11	0.54	-0.11	-0.19	-0.1	1.0
26	-0.73	-0.65	0.13	0.0	-0.17	-0.48	0.07	-0.15	-0.37	-0.34	-0.38	-0.17	0.23
27	-0.72	•••	•••	-0.31	-0.22	-0.61	0.02	-0.23	-0.27	-0.17	-0.65	-0.2	0.09
28	-0.7	•••	•••	-0.22	-0.29	-0.65	0.07	0.08	-0.52	-0.44	-0.54	-0.14	0.0
29	-0.67	-0.15	0.42	0.21	-0.18	-0.42	-0.04	0.04	-0.24	-0.21	-0.11	0.15	0.33
30	-0.63	-0.29	0.89	0.71	-0.1	-0.4	0.01	0.21	0.3	-0.04	-0.21		0.8
31	-0.55		•••	0.64	-0.05	•••	0.1	0.2	0.3	-0.14	-0.17	-0.17	0.7
32	-0.37				-0.07	•••	-0.15	0.23		-0.02	-0.13	-0.23	1.01
33	-1.59	0.43	1.17	1.22	-0.23		-0.03		0.32	•••		•••	0.68
34	-1.25	-0.38		0.96	-0.31	-0.25	-0.19	0.26		•••	-0.06	•••	•••
35	-1.67	•••	•••	1.24	0.04	-0.55	0.12	•••	0.38	•••	•••	•••	•••

			D.M.		0.6.77.3	F.4.100 3			rm: m 3		D ( T )	0.7.5	
#	[Fe/H]	[C/Fe]	[N/Fe]	[O/Fe]	[Mg/Fe]	[Al/Fe]	[Si/Fe]	[Ca/Fe]	[Ti/Fe]	[Cr/Fe]	[Mn/Fe]	[Ni/Fe]	[Ce/Fe]
36	-1.26			1.12	0.04	-0.59			0.32				•••
37	-1.92			0.74	-0.04	-0.46	0.36	0.43	0.05				
38	-1.47	-0.41	0.46	0.31	-0.24	-0.28	-0.03				-0.47		0.13
39	-1.7	0.04		0.41	-0.07	-0.53	0.11	0.41				-0.48	0.11
40	-1.67			0.6		-0.41	0.14	-0.02	0.04				0.28
41	-1.76	•••	•••	0.42	0.07		0.02	0.21		•••	•••	0.3	•••
42	-1.78			1.02	-0.13	-0.45	0.2					0.36	
43	-1.63			0.59	0.05		0.05	0.05					
44	-2.25			0.65	-0.07	-0.25	-0.1						•••
45	-2.17		•••	0.37	-0.01		0.19						0.39
46	-1.95	-0.04	•••	0.97	-0.09		0.03		•••	•••			•••
47	-1.74	-0.29	•••	0.72	0.03	-0.55	0.08		-0.35	•••			•••
48	-1.67			0.28			-0.32		-0.17			-0.43	-0.11
49	-1.18		•••	0.73	-0.01	-0.38	0.06	0.08	0.25		-0.08		0.07
50	-1.02		•••	0.59	-0.04	-0.48	0.04	0.17	0.12		-0.21		0.03
51	-1.19			0.84	0.23	-0.21	0.01	0.36	0.5		-0.06	-0.02	0.03
52	-1.51	•••	•••	0.39	-0.06		0.09	0.46	0.7	•••		•••	•••
53	-1.61			1.15	-0.14	-0.37	-0.03						0.26
54	-1.58	•••	•••	0.74	-0.02	-0.24	0.28	0.47	0.28	•••	•••	0.12	0.15
55	-1.75	-0.05	0.39	0.09	•••	-0.33	0.18	0.52	0.68	0.28	•••	-0.33	0.26
56	-1.81	-1.06	•••	-0.42	0.03	•••	0.39	0.11	0.19	•••	-0.29	-0.33	-0.15
57	-1.21	•••	•••	0.92		-0.09	0.11	•••	0.32	•••	-0.1	-0.09	0.56
58	-1.16		•••	1.15	-0.03	-0.65	-0.01		0.3	•••			-0.01
59	-1.54	-0.46	•••	0.44	-0.11	-0.51	0.19	0.25	-0.13	•••	-0.24	-0.36	0.18
60	-1.54		•••	0.17	0.05	-0.35	0.34	-0.04	0.73	•••	-0.24	-0.1	
61	-1.29	-0.2	•••	0.47		-0.5	0.09	-0.03	-0.16	•••	-0.03		0.13
62	-1.92	•••	•••	1.17			0.3		•••	•••	•••	0.35	-0.03
63	-1.25			1.17	-0.02	-0.28	0.09	0.21		•••		0.22	
64	-1.04	-0.34	0.34	0.65	-0.03	-0.41	0.18	-0.2	0.13	•••	-0.11	-0.02	0.06
65	-2.1 -1.96	 0.11	•••	0.51 0.13	0.24	-0.5	0.27 0.23	0.56	•••	•••	 -0.17	•••	0.19 0.18
66 67	-1.96		•••	0.13	 0.55	•••	-0.07	•••	-0.32	•••		•••	-0.08
68	-1.34 -1.99	 0.4	•••		-0.55 0.03	 -0.39	-0.07	•••		•••	•••	•••	
69	-1.99 -1.67	0.4	0.2	•••	-0.2		-0.03	•••	•••	•••	•••	•••	•••
70	-1.62			•••	-0.2 -0.45	•••	0.02	 0.17	•••	•••	•••	•••	•••
70	-1.02	•••	•••		-0.43 -0.54		-0.14	-0.08		•••	•••	-0.05	0.17
72	-1.57 -1.6	 -0.37	0.03	-0.31	-0.34 -0.71	-1.05	0.14	-0.08	-0.45		•••	-0.03 -0.47	-0.08
73	-1.44	-0.37	0.03	0.2	-0.71	-1.03	-0.13		-0.43			-0.47	0.25
73 74	-1.44	-0.47		0.2	0.11	-0.67	0.07		-0.14			-0.17	-0.07
	1.02	•••	•••	0.5	0.11	0.07	0.07	•••	0.52	•••	•••	0.07	0.07